UMTRI-94-24

SKIN BURNS FROM AIRBAG EXHAUST GAS: LABORATORY EXPERIMENTS AND MATHEMATICAL MODELING

FINAL REPORT

Matthew P. Reed
Lawrence W. Schneider

University of Michigan
Transportation Research Institute
2901 Baxter Road
Ann Arbor, Michigan 48109-2150

Submitted to:

Honda Research and Development North America
1990 Harper's Way
Torrance, California 90501

July 1994

Technical Report Documentation Page

1. Report No.	2. Government Accession No.	3. Recipient's Catalog No.
UMTRI-94-24		

4. Title and Subtitle	5. Report Date
SKIN BURNS FROM AIRBAG EXHAUST GAS: LABORATORY EXPERIMENTS AND MATHEMATICAL MODELING	July 1994
	6. Performing Organization Code
7. Author(s) Matthew P. Reed and Lawrence W. Schneider	8. Performing Organization Report No. UMTRI-94-24
9. Performing Organization Name and Address University of Michigan Transportation Research Institute 2901 Baxter Road Ann Arbor, Michigan 48109	10. Work Unit No. (TRAIS) 11. Contract or Grant No.
12. Sponsoring Agency Name and Address Honda Research and Development North America 1990 Harper's Way Torrance, California 90501	13. Type of Report and Period Covered FINAL REPORT 14. Sponsoring Agency Code

15. Supplementary Notes

16. Abstract

Although driver-side airbag systems provide protection against serious head and chest injuries in frontal impacts, injuries produced by the airbag itself have also been reported. Most of these injuries are relatively minor, and consist primarily of skin abrasions and burns. Previous investigations at UMTRI have addressed the mechanisms of airbag-induced skin abrasion. In the current research, laboratory studies related to the potential for thermal burns due to high-temperature airbag exhaust gas have been conducted. Measurements of airbag exhaust gas temperature and velocity were made during static airbag deployments. A laboratory apparatus was constructed to produce a 10-mm-diameter jet of hot air that could be directed onto the leg skin of human volunteers in time-controlled pulses. Skin burns were produced in 70 of 183 exposures conducted using air temperatures ranging from 350 to 550°C, air velocities from 50 to 90 m/s, and exposure durations from 50 to 300 ms. A mathematical model of heat transfer to the skin and burn injury was developed, along with an empirical description of the threshold for partial-thickness skin burns as a function of gas velocity, gas temperature, and exposure duration. The mathematical burn-injury model is combined with a lumped-parameter gas-dynamics model of airbag inflation to demonstrate the application of the skin thermal tolerance data to prediction of airbag-induced skin burn.

17. Key Words	18. Distribution Statement
Airbag, Thermal Burns, Injury Tolerance, Injury Mechanisms, Skin Injury, Restraint Systems, Modeling	Limited Distribution

19. Security Classif. (of this report)	20. Security Classif. (of this page)	21. No. of Pages	22. Price
None	None	68	

ACKNOWLEDGMENTS

The authors extend their thanks to Tomiji Sugimoto and Junichi Fukuda of Honda for their assistance with this project. Thanks also to Brooke Bowen for his assistance with the mathematical modeling, to Leda Ricci for her assistance in preparing this report, and to the eighteen people who volunteered for burn testing.

CONTENTS

LIST OF TABLES

LIST OF FIGURES

1.0 INTRODUCTION

Skin burns produced by airbag deployment have been reported by several crash investigation teams (Huelke *et al.* 1993; Reinfurt *et al.* 1993). Most airbag-induced burns are first or second degree (partial-thickness skin loss) and are found on the hands and forearms of drivers. Thermal burns due to passenger-side airbag deployment have not yet been reported. The incidence of thermal burns due to airbag deployment is difficult to determine, partly because of other potentially airbag-related injuries that may be misclassified as burns. Abrasions caused by the deploying airbag fabric are sometimes characterized as burns, although the injury mechanism is mechanical rather than thermal. In a survey of 215 crash survivors protected by driver-side airbags, 28 percent of those interviewed reported being injured by the airbag (Reinfurt *et al.* 1993). Twenty-six percent of respondents who reported being injured by the airbag said that their most severe injury was a burn. Although this database is small and self-reported, it suggests that skin burns are a substantial percentage of airbag-induced injuries.

There are two potential sources of thermal injury to the skin during and after an airbag deployment. First, the hot gas that inflates the airbag may cause burns if the gas impinges on the skin as it is exhausted through the vent ports at the back of the airbag. Burns from this source are likely to be first or second degree and are caused by convective heat transfer. Second, burns can be caused by skin contact with the metal inflator housing, which is extremely hot for several minutes after the deployment. Contact with the inflator will cause third-degree burns almost instantaneously because of the high temperature of the metal inflator housing and the high rate of heat transfer to the skin with contact. The occupant is protected from inflator contact to some extent by the airbag fabric and the module cover, but an occupant who pushes the deflated airbag out of the way with his or her hands, or attempts to stuff the airbag back into the module, may touch the inflator and be burned. The latter type of burn due to contact with the inflator, while more severe, is probably less common than burns due to heat transfer from the hot inflation gas.

The research described in this report addresses only burns due to hot gases impinging on the skin. Conduction burns due to contact with hot airbag components and burns due to failure of airbag components (*e.g.*, fabric rupture) are not considered. The objective of this research was to determine if airbag exhaust gas can cause skin burns, and, if so, to develop an engineering tool that can assess the potential of airbag systems to cause burns. The research proceeded in three phases:

Phase 1: Measure Temperature and Velocity of Airbag Exhaust Gas

Phase 2: Determine Human Skin Sensitivity to Convection Burns

Phase 3: Predict Airbag-Induced Skin Burn by Integrating an Airbag Inflation Model with a Mathematical Skin-Burn Model

A fourth phase was originally planned to develop a laboratory technique for evaluating the burn injury potential of airbags, but the research demonstrated that the model developed in Phase 3 is a better method of assessing burn potential of airbags.

Three report sections follow this introduction. Section 2 presents the results of testing to characterize the convective thermal insult posed by airbag exhaust gas. Section 3 describes the apparatus and methods used to determine the sensitivity of human skin to high-temperature, high-velocity, air-jet exposures. In Section 4, two mathematical models are described. The burn injury model describes heat transfer to the skin from an impinging gas jet and provides a prediction of burn injury. An airbag inflation model is used to obtain predictions of airbag exhaust gas temperature and velocity, which are used with the burn injury model to assess the burn injury potential of particular airbag module designs. The complete mathematical model formulations, and example calculations with intermediate results, are in the appendices.

2.0 MEASUREMENT OF THE TEMPERATURE AND VELOCITY OF AIRBAG EXHAUST GAS

Convection heat transfer to the skin during deployment of an airbag with nonporous fabric is affected by the temperature, velocity, and composition of the airbag exhaust gas exiting the vents, as well as by the geometry of gas jet and skin surface. The gas produced by sodium azide inflators is predominantly nitrogen. The exhaust gas jet from a typical airbag vent can be reasonably approximated by a circular jet, although the geometry of the target surface, and its orientation relative to the gas jet, can be expected to vary widely in field deployments. The temperature and velocity of the airbag exhaust gas are the two most important variables for determining the heat transfer coefficient and the rate of heat transfer. Therefore, laboratory experiments were conducted in an attempt to measure the exhaust gas temperature and velocity for several different airbag inflators, using driver-side airbags with coated (nonporous) fabric.

2.1 AIRBAG EXHAUST GAS TEMPERATURE MEASUREMENT

The exhaust gas temperature was measured during static deployments by 0.0005-inch (0.0127-mm), Type-K thermocouples placed in the gas stream as shown in Figure 1. The tethered, 60-L airbag, with two 38-mm vent ports, was mounted unfolded to the test fixture. The thermocouples were mounted adjacent to the vent ports to record the temperature of the escaping gas. The thermocouples were constructed using thermocouple junctions, ceramic insulators, and connectors from Omega, Inc. The thermocouple assemblies were connected electrically to linearizers from Omega, Inc., which convert the thermocouple voltage to a 1-mv/°C signal. The linearizer output was recorded using A/D hardware and software.

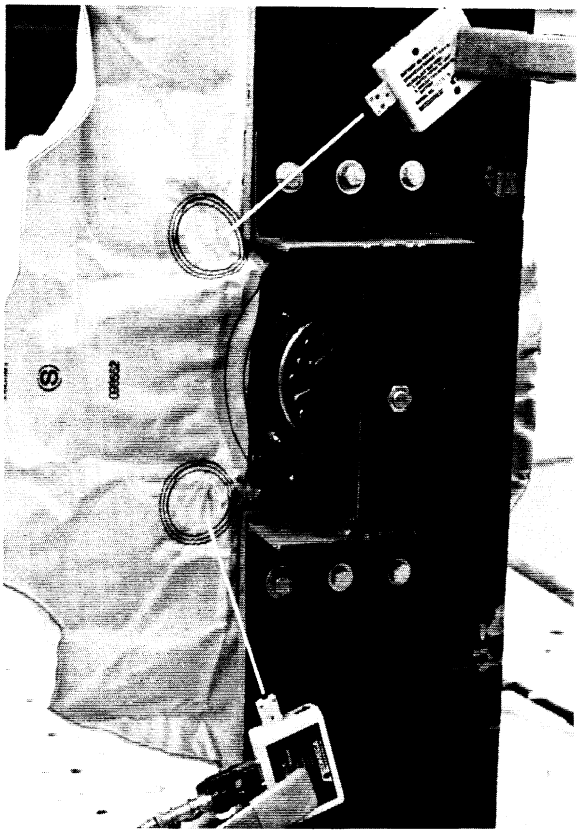

Figure 1. Test fixture for measuring airbag exhaust gas temperature.

Figure 2 shows a typical temperature recording made during a deployment with a 350-kPa inflator. Table 1 shows typical peak temperatures from tests with five different inflators. These peaks were estimated visually to the nearest 50 °C, using data from several tests with each inflator. Peak exhaust gas temperature is correlated with inflator capacity. There was wide variability in the data, both between tests with nominally identical inflators and between exhaust ports during the same test. A substantial amount of this variability was probably due to the difficulty in positioning the thermocouples consistently in the gas stream.

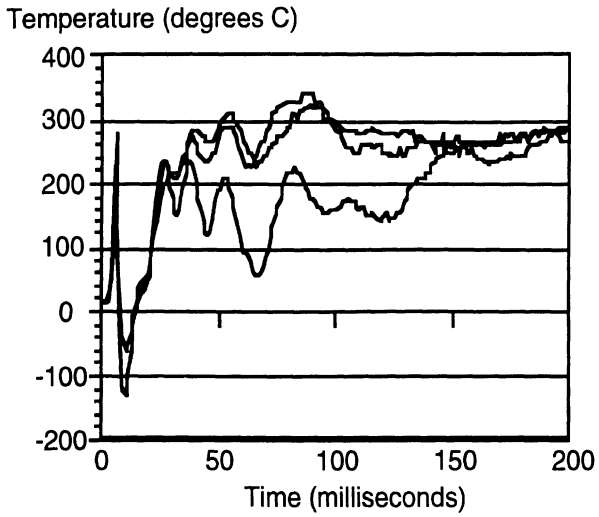

Figure 2. Typical temperature data obtained from a deployment with a 350-kPa inflator. Top two traces are data from two thermocouples at one vent port. Bottom trace is from a thermocouple at the other vent port during the same deployment.

Table 1
Typical Peak Exhaust Gas Temperatures

Inflator Capacity (kPa)	Peak Temp °C
320	200
350	300
420	400
475	450
560	500

The initial spike in the temperature data shown in Figure 2 is apparently due to a small puff of exhaust gas that exits the vent ports immediately after the inflator is ignited. This burst of gas is visible in the high-speed films of these deployments. The subsequent negative-going temperature spike has not been explained but was observed in almost all tests. Two possible explanations have been advanced. First, oscillations in the linearizers or data acquisition equipment may have produced this spike following the initial burst of gas from the inflator. However, similar trends were observed when the

thermocouples were sampled without the linearizers, and efforts to induce the effect by introducing step temperature changes were unsuccessful. A second possible explanation is that the local pressure in the area of the thermocouple is reduced substantially by the deploying airbag, thereby reducing the local temperature. When the airbag is deployed from this test configuration, the airbag snaps rapidly forward from its initially flat position, away from the thermocouples. This motion may create a local reduction in pressure that would lower the gas temperature. However, these negative-going temperature peaks occasionally reached impossibly cold temperatures (*e.g.*, below –300 °C), suggesting that instrumentation artifacts were at least partially responsible for these unexpected data.

The oscillations in the temperature data observed after about 25 ms correlate well in frequency with the oscillatory motions of the airbag. Periods of peak temperature correspond to periods of the deployment in which gas was streaming more steadily from the vent ports, while valleys in the temperature curves were observed when the airbag rebounded away from the thermocouples and only small amounts of escaping gas were observed on the high-speed film. In previous testing, the internal pressure of the airbag was found not to show substantial oscillation during the later phases of the deployment, suggesting that the movement of the airbag results in volume changes, venting excess gas each time the volume is reduced by the airbag movement. The valleys of the temperature measurement data correspond to periods of low gas flow when the gas at the thermocouple location has entrained more room air and is consequently at a lower temperature.

2.2 AIRBAG EXHAUST GAS VELOCITY MEASUREMENT

Several tests were conducted in an attempt to measure the velocity of the airbag exhaust gas. Small foam beads were placed in an unfolded airbag prior to deployment. High-speed film of the area around the exhaust ports was recorded at 6000 frames per second. The film was analyzed to determine the velocities of the foam beads as they were expelled from the airbag. Although there was considerable variability, pellet velocities between 100 and 200 m/s were measured for an airbag with a 350-kPa inflator. The method did not appear suitable for accurate measurement of exhaust gas velocity because of the high variability and the unknown relationship between the foam-bead velocities and the actual mean gas velocity.

Because of the problems in measuring accurately both the temperature and velocity of the airbag exhaust gas, a new method of characterizing the nature of the thermal insult produced by airbags was developed. A mathematical gas-dynamics model describing the airbag inflation process was constructed, based on a formulation published by Wang and Nefske (1988), Wang (1989), and Wang (1991). The model predicts the temperature and velocity of the gas exiting the airbag exhaust ports from the airbag specifications and the tank-test performance of the inflator. This model is described in detail in Section 4.

3.0 BURN THRESHOLD FOR HUMAN SKIN EXPOSED TO HIGH-TEMPERATURE, HIGH-VELOCITY AIR JET

3.1 APPARATUS

A laboratory "heat gun" was developed to produce a 10-mm-diameter jet of air at prescribed temperatures and velocities. Figure 3 shows the heat gun. The heat gun is capable of producing temperatures up to 550 °C and velocities up to 100 m/s (depending on temperature). Electromechanical shutters are used to control the exposure duration. An electronic timing box sequences the shutters to provide the desired exposure duration. High-speed film of the shutter operation showed that each shutter takes 25 ms to swing completely across the 30-mm opening in the shutter-mounting plate. Since the gas jet is only 10 mm in diameter, the time during which the jet is partially blocked is substantially less than 25 ms. Since the two shutters move in the same direction, each section of the target area is exposed for the same period of time. The high-speed film confirmed that the timing box and shutters produced the desired exposure durations to within 2 ms.

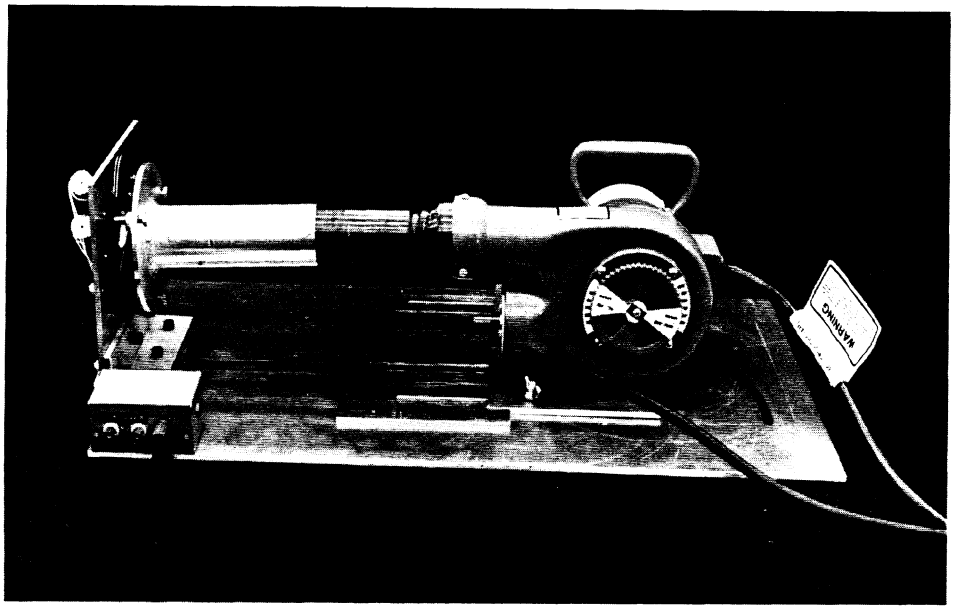

Figure 3. Heat gun used to produce controlled convection exposures.

Heat gun temperatures were measured at the exhaust port. The temperature probe contained a Type-K thermocouple located in the center of a 10-mm-diameter port. The probe was fitted over the end of the heat gun to measure the gas temperature. Because of the high temperatures produced by the heat gun, errors in measurement due to conduction along the thermocouple wires and radiation from the thermocouple to the surrounding

metal were likely. However, measurements made with other thermocouple arrangements, including the fine-gage thermocouples used in airbag testing, suggested that the measured temperatures were accurate to within about 10 °C. Zero point and boiling point values were verified to within 1 °C with each thermocouple prior to use.

Heat gun air velocities were measured during testing with an Omega, Inc. hot-wire anemometer. With the anemometer in place, the air velocity was varied by adjusting the AC voltage supplied to the blower using a Variac, Inc. variable transformer. The anemometer provided a reasonably quick, repeatable measurement of gas jet velocity. However, the accuracy of the measurement was suspect because of the large probe diameter relative to the gas jet. Further, the anemometer could be used only at ambient temperatures (*i.e.*, 20 to 25 °C). A pitot tube was constructed to obtain a more accurate measurement of velocity.

First, the hot-wire anemometer was used to set the blower at the voltage used for each of the three nominal velocity test conditions (30, 40, and 50 m/s). The differential pressure across the pitot tube was then measured at ambient temperature (20 to 25°C) and at 50 °C increments to 550 °C, using a water manometer. At each nominal velocity setting, the differential pressure was found to increase by a few mmH_20 between 20 and 300 °C, and then to remain constant up through 550 °C. This constant differential pressure for each nominal velocity condition, along with the gas temperature, produced a unique test velocity for each test condition. The actual velocity was calculated from the pitot tube formula

$$V = \sqrt{\frac{2\,\Delta P}{\rho}}\,, \qquad (1)$$

where v is the gas velocity, ΔP is the differential pressure across the static and dynamic ports of the pitot tube, and ρ is the air density, calculated as a function of temperature. At ambient temperature, the pitot-tube calculated velocity is about 15 percent higher than the anemometer-measured velocity.

3.2 PROCEDURES

Tests were conducted at 14 different temperature/velocity combinations, using the leg skin of male volunteers 20 to 32 years of age. The hair on the subjects' legs was shaved with an electric razor prior to testing. Subjects were fully informed as to the nature of the testing and consent was obtained in writing.* At the start of a series of trials, the heat gun temperature and velocity were set to desired levels. Three nominal velocity levels were chosen: 30, 40, and 50 m/s. The actual velocity was determined by the nominal velocity, set at ambient conditions, and the subsequent temperature setting. For example, the test condition with a nominal velocity of 30 m/s and 400 °C had an actual velocity of 64 m/s, measured by the pitot-tube method described above. The nominal velocity levels were set during testing by adjusting the input voltage to the heat gun blower, using the hot-wire anemometer to monitor the velocity. Subsequent to testing, the actual velocity at each of the test conditions was measured using a pitot tube.

---

* The rights, welfare, and informed consent of the volunteer subjects who participated in this study were observed under guidelines established by the U.S. Department of Health, Education, and Welfare (now Health and Human Services) on Protection of Human Subjects and accomplished under medical research design protocol standards approved by the Committee to Review Grants for Clinical Research and Investigation Involving Human Beings, Medical School, The University of Michigan.

The subject's leg was placed against the protective screen as shown in Figure 4 so that only a 50-mm-diameter area of skin was exposed. The exposure duration was initially set to a level below that believed to be necessary to cause a burn. Each subsequent exposure was conducted on a different area of skin, with the exposure duration increased by 10 ms each time. The burn threshold for a particular temperature/velocity combination was defined as the duration midway between the longest exposure that did not result in a burn and the shortest exposure that produced a second-degree burn. Each subject participated in a maximum of 10 exposures. Assessment of injury was made 48 to 72 hours after exposure. An exposure was categorized as producing a burn if the exposed area showed regions of discoloration that did not blanch with 5 seconds of firm pressure, indicating cell death.

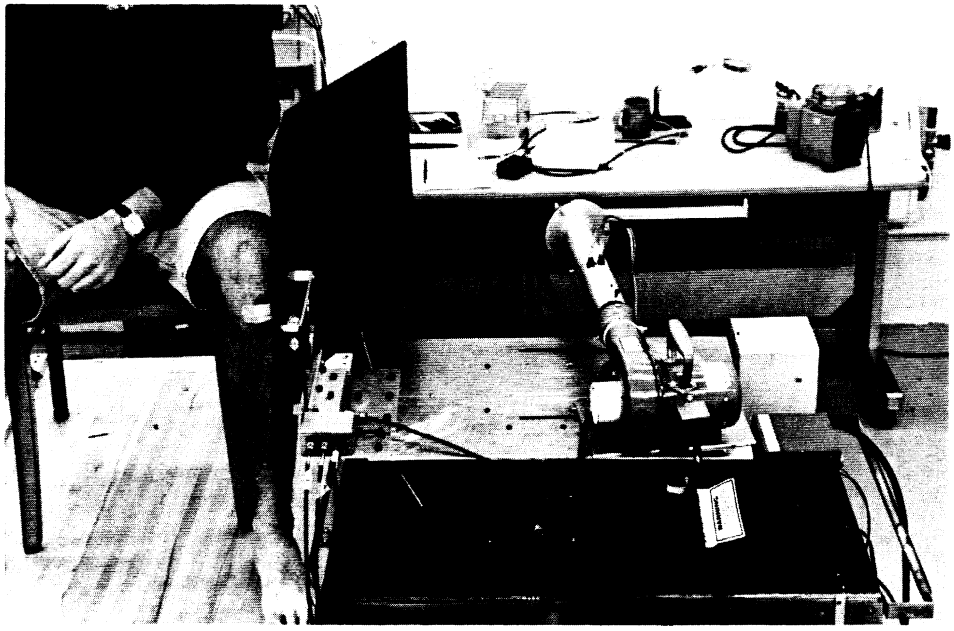

Figure 4. Heat gun with subject positioned for testing.

3.3 RESULTS OF HUMAN SUBJECT TESTING

Figure 5 shows several burns produced by the heat gun. Most of the burns observed were circular and 15 to 20 mm in diameter, although in some cases near the threshold duration the burns were irregularly shaped and covered a smaller area. This irregularity was probably due to local variations in epidermal thickness. Figure 6 and Table 2 show the threshold durations obtained for 14 test conditions. The solid lines in Figure 6 connect data obtained at each of the three nominal test velocities. The numbers adjacent to each point indicate the actual test velocity calculated using pitot-tube data.

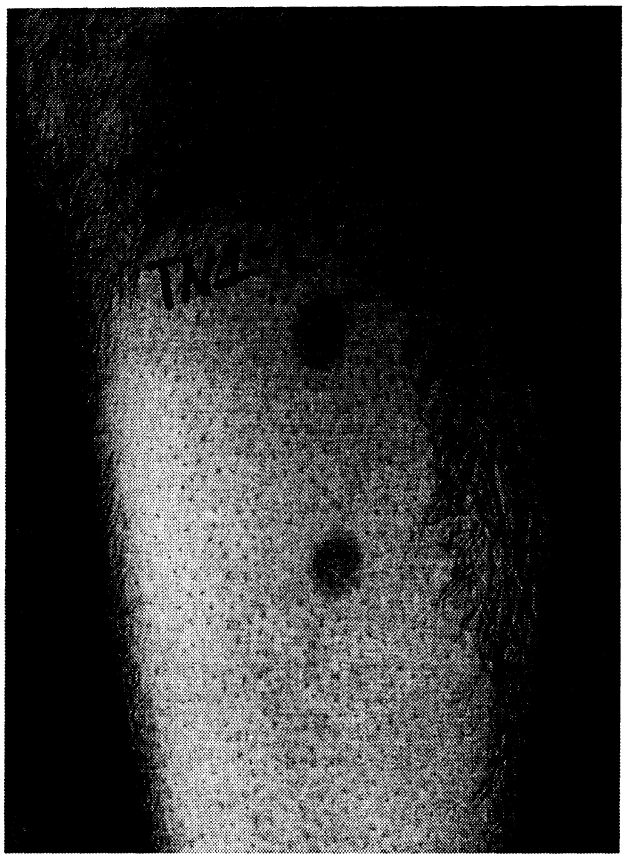

Figure 5. Photo of subject's leg taken 72 hours after exposure, showing two areas of convection burn produced by the heat gun.

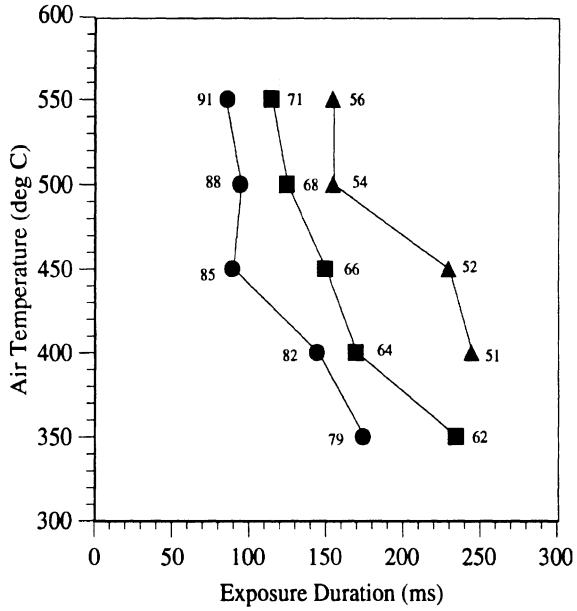

Figure 6. Exposure-duration thresholds for 14 temperature-velocity conditions using the laboratory heat gun. Lines connect nominal velocity conditions: ▲ = 30 m/s, ■ = 40 m/s, ● = 50 m/s. Numbers next to each data point indicate actual air velocities.

Table 2
Tabulated Exposure-Duration Thresholds in Milliseconds
for Partial-Thickness Burns Using the Laboratory Heat Gun

Air Temperature (°C)	Nominal Velocity†		
	30 m/s	40 m/s	50 m/s
350	--	235 (62)	175 (79)
400	245 (51)	170* (64)	145 (82)
450	230 (52)	150* (66)	90 (85)
500	155 (54)	125 (68)	95 (88)
550	155 (56)	115 (71)	85 (91)

† Actual velocities are shown in parentheses.
* Threshold is average from two subjects. All other thresholds were determined with data from only one subject.

The exposure duration threshold versus temperature for the 10-mm-diameter heat gun was found to be described well by an exponential equation,

$$t = \text{Exp}[\, 8.03 - 0.0263\, u - 0.00381\, T + 1.642 \times 10^{-5}\, uT \,] \qquad (2)$$

where t is the threshold expressed in milliseconds, u is the gas velocity in m/s, and T is the gas temperature in °C. The equation was obtained by a least-squares fit of a linear equation with one interaction term to the logarithm of the threshold data from Figure 6. Figure 7 shows the surface described by equation (2), along with lines corresponding to the test conditions used in human-subject testing. Figure 8 shows a comparison of equation (2) with the threshold data.

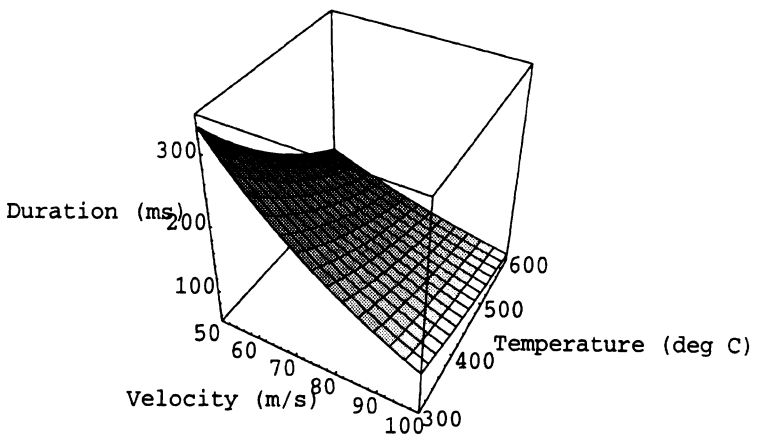

Figure 7. Relationship between temperature, velocity, and threshold exposure duration for the heat gun, based on equation (2), an exponential fit to the data.

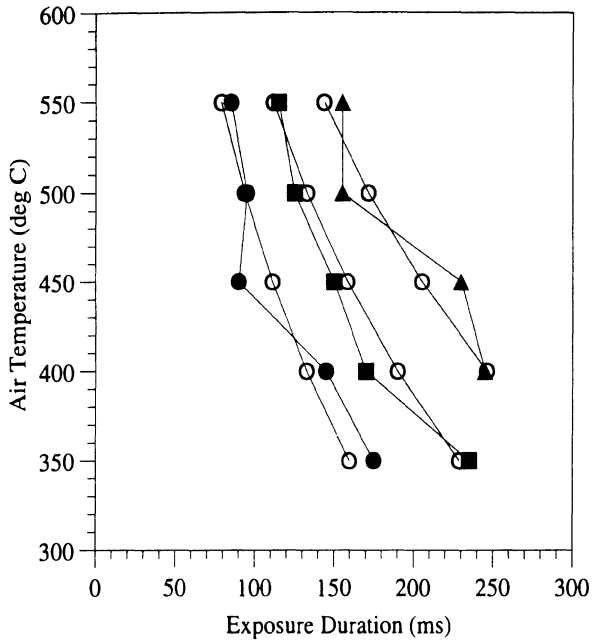

Figure 8. Exponential fit to threshold data. Data from heat gun tests are shown as in Figure 6. Threshold predictions for each of the test conditions obtained using equation (2) are shown with O symbols.

Two expected trends were observed in the human burn threshold data. First, increasing velocity decreased the exposure duration necessary to produce a second-degree burn. Second, increasing temperature also decreased the threshold exposure duration. The effect of increasing temperature on the threshold duration decreased with increasing temperature. At high velocities, the effect of changing the temperature from 300 to 600 °C has only a small effect on the threshold exposure duration (see Figure 7).

The data shown in Figure 8 do not represent constant velocity curves, because each data point was obtained at a different velocity. Figure 9 shows constant-velocity threshold curves obtained using equation (2).

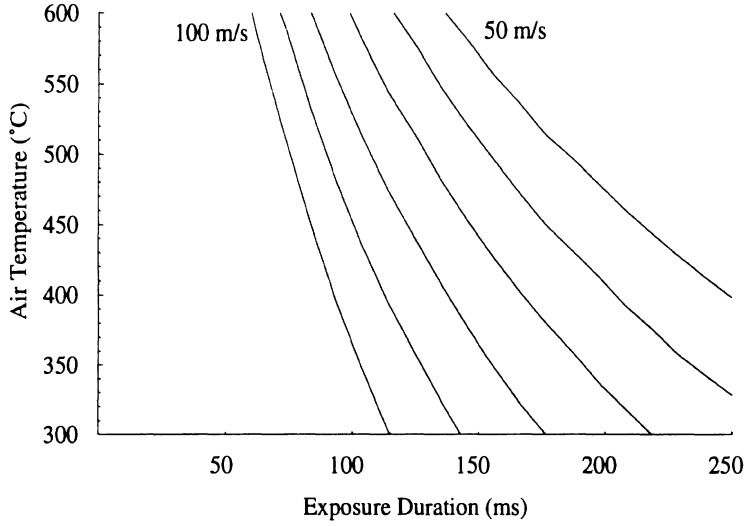

Figure 9. Constant velocity curves obtained using the exponential fit to the heat gun data. From right to left are curves for 50, 60, 70, 80, 90, and 100 m/s.

4.0 MATHEMATICAL MODELS TO PREDICT BURN INJURY FROM AIRBAG DESIGN PARAMETERS

4.1 BURN INJURY MODEL

A mathematical description of the sensitivity of the skin to burn injury is desirable for several reasons. First, extrapolating the experimental data of Section 3 to other conditions of interest is best performed using a model that accurately reflects the state of knowledge concerning burn sensitivity. Second, a model can be used to predict the effects of parameters not previously investigated, *e.g.*, gas properties or skin thickness.

Two types of models have been constructed. Equation (2) represents an empirical model that predicts the exposure duration threshold as a function of air velocity and temperature. This simple empirical model represents a reasonable statement of the burn threshold for air, using a 10-mm-diameter, perpendicularly impinging, gas jet, over the range of velocities and temperatures investigated. It cannot, however, be used to extrapolate these results to substantially different gas compositions and different gas jet geometries, or to estimate the effects of skin thickness variability on the threshold. To accomplish the latter objectives, an analytical model of skin burn was developed, drawing heavily on the work of two Harvard University researchers who conducted in-depth investigations of the sensitivity of human and porcine skin to burn injury by conduction and passive convection. Several key components of their work are incorporated in the current model.

4.1.1 Background

The most important and thorough work on human sensitivity to skin burn was conducted nearly five decades ago, by researchers Henriques and Moritz of Harvard University. In four papers (Henriques 1947, Henriques and Moritz 1947, Moritz 1947, Moritz and Henriques 1947) they describe experiments with pigs and human volunteers to determine the skin temperatures and exposure durations necessary to produce burns. Their experiments were primarily concerned with conduction burns, that is, burns produced by direct contact between the skin and a hot object. Burns were produced experimentally using hot metal blocks and by application of flowing hot oil and water. An important assumption of their work is that the application of a hot object to the skin surface immediately brings the surface temperature of the skin to the temperature of the contacting object. This assumption has high validity for the range of exposure durations investigated, which ranged from one second for high temperatures to eight hours for lower temperatures. The most important contribution of this work was the development of a mathematical model to describe heat transfer into the skin and the formulation of an burn injury criterion function that modeled thermal cell injury as a rate process.

4.1.1.1 Skin Anatomy and Burn Classification. The anatomy of the skin is an important starting point for the discussion of thermal injury. Figure 10 shows a schematic of the skin, which is comprised of two layers: the epidermis and the dermis. The outer layers of the epidermis are comprised of dead, dry cells that form a protective covering for the underlying tissues. The lowest layers of cells in the epidermis are alive, but die and dry out while gradually migrating toward the surface as the outer cells are sloughed off. The dermis is much thicker than the epidermis, consists of a variety of living cells, and includes sweat glands and hair follicles.

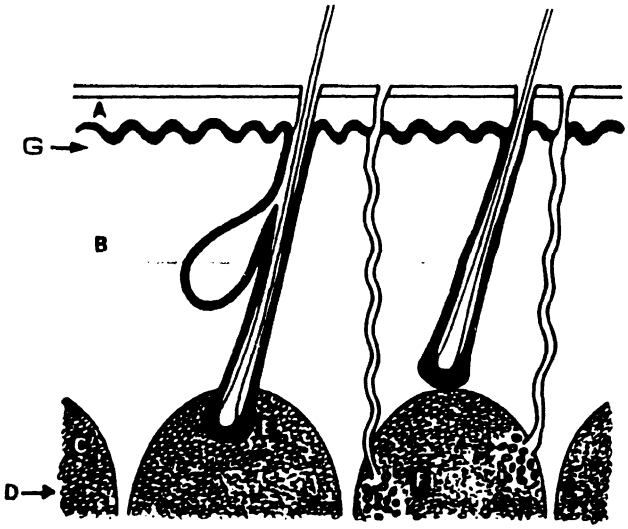

Figure 10. Schematic cross-section of human skin. Epidermis (A) is much thinner than the dermis (B). Hair follicles (E) are implanted in the lower dermis or a dome of underlying fat (C). Sweat glands are located deeper (F). The junction between the epidermis and dermis (G) is the most superficial level at which burn injury can occur. Burns with cell necrosis penetrating between G and D are partial-thickness burns, with greater severity associated with greater depth of necrosis. Burns involving the entire dermis to the depth D are full-thickness burns (from Zawacki 1987).

During a burn event, the first cells to be damaged are those in the most superficial living layer that are alive, namely, the basal layer of epidermis. As the length of exposure is increased, or the rate of heat transfer to the skin increases, the depth of cell damage increases. It is customary to classify burns according to degree (*e.g.*, first degree, second degree, third degree). A first-degree burn is characterized by redness that fades in a few days. A second-degree burn usually produces blistering and peeling of skin. A third-degree burn has a surface appearance of charred or gray flesh immediately after exposure, indicating immediate cell death in the outer layers of skin. One problem with this classification system is that the rate of heat transfer to the skin and the exposure duration determine the severity of the burns within each classification. A third-degree burn may be less severe physiologically than a second-degree burn if the depth of cell necrosis with the third-degree burn is less than for the second-degree burn.

A more useful classification is based on the skin thickness to which cell death progresses (Zawacki 1987). A first-degree burn is characterized by erythema, or reddening, which indicates that the skin is irritated but no cells have been destroyed. This is a burn without skin loss. A partial-thickness burn is a burn where cells have been destroyed, but less than the entire thickness of epidermis and dermis has been affected. The most superficial partial-thickness burn affects only the outermost layer of living cells, that is, the basal epidermal layer. More serious partial-thickness burns affect the dermis. A burn is described as full-thickness when cell death has progressed through the entire thickness of epidermis and dermis. Such burns are serious and grafting is usually required.

The ambiguity of the customary classification system is now apparent. A second-degree burn (with blistering and skin cell loss) can involve only the outermost layers of living tissue, or may involve the full dermis, which results in a much more severe burn. Similarly, a third-degree burn (charred or gray surface) can be superficial (partial or no skin loss) if the heat transfer is at a very high rate for a very short period of time. The duration of healing, the potential for scarring, and the need for medical care are all related to the depth of injury, so using the partial/full skin loss classification is generally more useful.

The threshold for burn injury of current interest is defined as the condition that results in cell necrosis (death) at the most superficial level of living tissue; that is, the least severe burn that results in skin (epidermis) loss. The basal epidermal layer is the critical skin depth for partial thickness burn. Other thresholds could be calculated for various depths of injury, including full-thickness burn.

For a range of exposure durations from one second to eight hours, Henriques (1947) plotted the minimum skin surface temperature necessary to cause full *epidermal* thickness (minimum-severity partial skin loss) burns in pigs and human subjects. These data are replotted in Figure 11. Note that as the surface temperature increases, the exposure duration required to produce a burn decreases rapidly (time axis in Figure 11 is logarithmic). A skin surface temperature of about 45 °C can be sustained almost indefinitely without burn injury, while a skin surface temperature of 70 °C will kill cells at the basal epidermal layer with exposure of only one second.

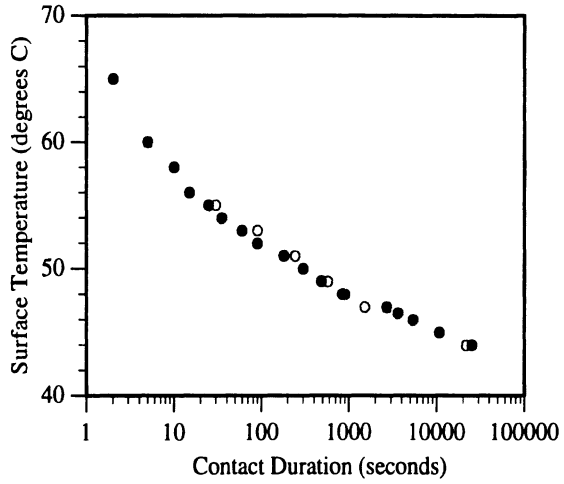

Figure 11. Contact exposure duration thresholds for transepidermal necrosis in pig skin (●) and human skin (O), from Moritz and Henriques (1947).

4.1.1.2 Semi-Infinite Solid Heat Transfer Model. In order to describe the process of burn injury taking place within the skin, Henriques and Moritz first developed an analytical method to predict the temperature within the skin as a function of the surface temperature, skin parameters, and time. They chose to model the skin and underlying tissue as a semi-infinite solid, that is, a homogeneous solid of infinite depth and breadth exposed uniformly on its surface to a heat source. The problem is then one-dimensional conduction perpendicular to the surface. The temperature distribution within a semi-infinite solid can be obtained by solving the Fourier heat equation with the appropriate boundary and initial conditions. For one dimension, the heat equation is

$$\frac{\partial^2 T}{\partial x^2} = \frac{1}{\alpha_s}\frac{\partial T}{\partial t}, \tag{3}$$

where T(x, t) is the skin temperature at depth x and time t, and α_s is the thermal diffusivity of the skin. The Fourier equation indicates that the rate of change of temperature at a particular skin depth is proportional to the second derivative of the temperature distribution, or, equivalently, the rate of change of the temperature gradient with x. Under steady state conditions, $\frac{\partial T}{\partial t}$ is zero, so the second derivative of the

temperature distribution over x is also zero, indicating that the temperature distribution is linear. Under transient conditions, $\frac{\partial^2 T}{\partial x^2}$ is non-zero and the temperature at each x changes with time.

The thermal diffusivity is

$$\alpha_s = \frac{k}{\rho c_p} \tag{4}$$

where k is the thermal conductivity, ρ is the density, and c_p is the heat capacity of the skin. Henriques and Moritz (1947) obtained both epidermal and dermal values of k and c_p for pig skin. According to their research and more recent work (Meyer *et al.* 1978), pig skin is similar in these characteristics to human skin. Using a value of 0.8 g/cm^3 for the density of the skin, they demonstrated that the Fourier equation with the k, c_p, and ρ values obtained for epidermis produced accurate predictions of temperatures within the skin during the transient phase of conduction, as measured by embedded thermocouples.

Henriques and Moritz used a closed-form solution of the heat equation for a constant initial temperature over x (depth), and a constant skin surface temperature for $t > 0$. An equivalent formulation from Incropera and DeWitt (1985) is

$$\frac{T(x, t) - T_i}{T_i - T_s} = \theta\left(\frac{x}{2\sqrt{\alpha t}}\right), \tag{5}$$

where T_i is the initial skin temperature (constant over depth), T_s is the skin surface temperature, and θ is the Gaussian error function

$$\theta(w) \equiv \frac{2}{\sqrt{\pi}} \int_0^w e^{-v^2}\, dv. \tag{6}$$

Using equation (5), Henriques and Moritz calculated the temperature history at the basal epidermal depth for each skin surface temperature in their experiments. The basal epidermal depth was estimated from measurements on pig skin to be about 80 µm below the skin surface. Recent measurements of epidermal thickness (Falstie-Jensen *et al.* 1988) found similar values, with an average of 72 µm for the leg skin near the region tested with the heat gun in the current study.

4.1.1.3 Injury Criterion Function. To predict burn injury, the relationship between the temperature history at the critical skin depth, obtained by equation (5), and the likelihood of transepidermal burn was examined. Henriques (1947) observed that burn injury exhibits some of the key characteristics of chemical rate processes. There exists some threshold temperature below which the process does not occur, an "activation energy." Above this temperature, the process occurs at an accelerated rate with higher temperatures. A typical differential formulation of a rate process is

$$\frac{d\Omega}{dt} = G\, \mathrm{Exp}\left[\frac{-\Delta E}{R\, T(t)}\right], \tag{7}$$

indicating that the rate of change of some parameter of interest, Ω, is proportional by G, a constant, to an exponential function of ΔE, the activation energy (a constant characteristic of the process), R (the ideal gas constant), and T(t), the temperature as a function of time. The use of the ideal gas constant in the equation gives ΔE the units of J/mol.

Examination of equation (7) shows that $\frac{d\Omega}{dt}$ will be large and positive when the temperature is high, and that below some threshold temperature, the Ω process (burn injury) will proceed very slowly. To obtain Ω directly, equation (7) can be integrated over time to give

$$\Omega = G \int_0^t \mathrm{Exp}\left[\frac{-\Delta E}{R\,T(t)}\right] dt\,. \tag{8}$$

The threshold data on transepidermal injury obtained by Henriques and Moritz were used to determine appropriate values for the constants G and ΔE in equations (7) and (8). Data from trials with skin surface temperatures below 50 °C were selected, because in those trials the temperature gradient in the epidermis was sufficiently small during most of the exposure that the basal epidermal temperature could reasonably be taken to be constant and equal to the skin surface temperature. Exposure durations resulting in threshold-level second-degree burns were approximately 300 seconds at 50 °C. For constant temperature, equation (8) integrates to

$$\Omega = G\,t\,\mathrm{Exp}\left[\frac{-\Delta E}{R\,T}\right] \tag{9}$$

where T is the constant cell temperature.

The threshold data consist of temperature/time pairs corresponding to the threshold for transepidermal burn. Eight data points were used in the analysis. Henriques (1947) arbitrarily assigned $\Omega = 1$ to correspond to transepidermal necrosis and calculated the parameters G and ΔE using graphical fitting techniques. The values identified by Henriques are

$G = 3.1 \times 10^{98}\ s^{-1}$, and

$\Delta E = 629 \times 10^3$ J/mol.

The value of R used by Henriques (1947) was 2 cal/mol/K, or 8.374 J/mol. A more accurate value of R (Incropera and DeWitt 1985) is 8.3144 J/mol/K. In equation (9), the coefficient of T is $1/(\Delta E/R)$, so the appropriate value of ΔE is dependent on the value of R used. Taking R as 8.3144 J/mol/K, the recalculated parameter values are

$G = 3.1 \times 10^{98}\ s^{-1}$, and

$\Delta E = 623580$ J/mol.

Because of the importance of these values in predicting the burn thresholds, the data used by Henriques were tabulated from their papers (Henriques and Moritz 1947, Henriques 1947) and a new fit was performed using a least-squares procedure. Although the parameter values obtained are numerically slightly different, the predicted threshold exposure durations are nearly identical. Consequently, the recalculated parameter values given above were used.

4.1.2 Adaptation of the Henriques and Moritz Burn Injury Model

The thorough work of Henriques and Moritz formed a firm foundation for the current research. As a starting point for the current modeling effort, the most important aspects of their study were:

(1) determination of skin thermal properties,
(2) validation of the semi-infinite solid heat transfer modeling assumption, and
(3) demonstration of a rate-function model of the burn injury process.

The primary differences between the previous and current research are:

(1) Henriques and Moritz used conduction and passive convection in their experiments. Forced convection at the skin surface due to airbag exhaust gas imposes different boundary conditions.

(2) The shortest contact exposure produced by Henriques and Moritz was one second. In contrast, the exposure durations associated with airbag exhaust gas are generally less than 250 ms.

To add a forced-convection component to the model, an appropriate means of calculating the heat transfer coefficient due to an impinging gas jet was required. The relatively short exposure durations and high gas temperatures necessitated addition of a second phase to the heat transfer model with different boundary conditions.

4.1.2.1 Calculation of Convection Heat Transfer Coefficient. The exhaust gas exiting the airbag at an exhaust port and striking the skin surface is modeled as a round gas jet impinging perpendicularly onto an infinite plane surface, as shown schematically in Figure 12. Although many other impingement conditions may occur in the field, the perpendicularly impinging jet produces the highest heat transfer rate and is consequently a conservative assumption.

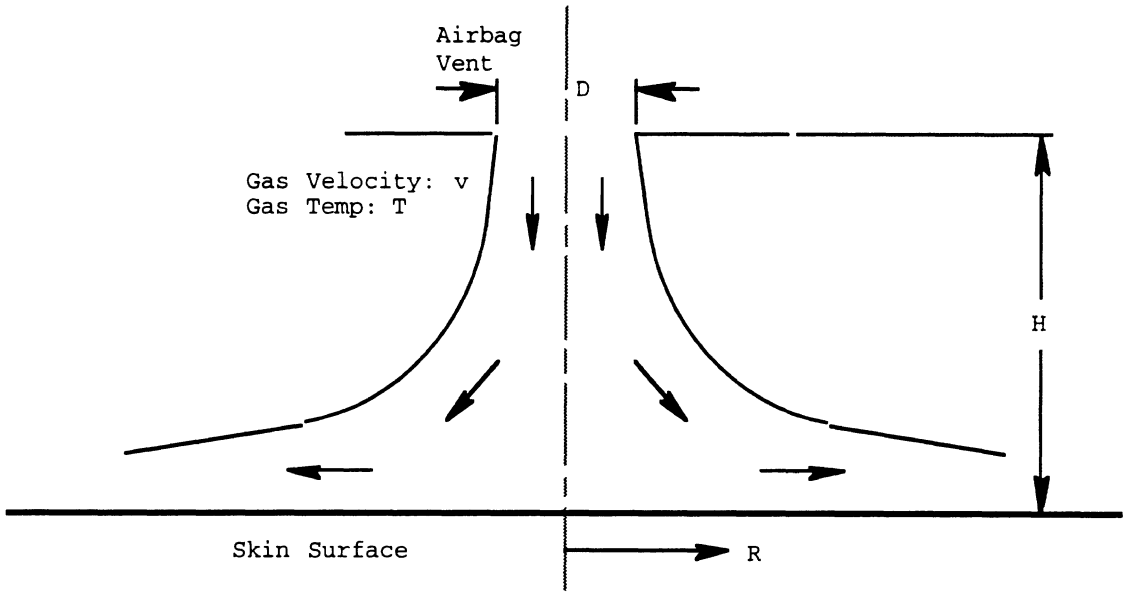

Figure 12. Schematic of impinging gas jet.

Martin (1977) has reported empirical correlations relating the Reynolds number (Re) to a ratio of Nusselt (Nu) to Prandtl (Pr) numbers. These dimensionless parameters are defined as follows:

$$Re = \frac{uD}{\nu} \tag{10a}$$

$$Nu = \frac{hD}{k} \tag{10b}$$

$$Pr = \frac{\nu_f}{\alpha} \tag{10c}$$

where

u is the gas jet free-stream velocity,
r is the radius of target area,
D is the vent diameter,
ν_f is the kinematic viscosity of the gas evaluated at the film temperature,
k is the thermal conductivity of the gas,
h is the heat transfer coefficient from the gas to the surface, and
$\alpha = \frac{k}{\rho c_p}$, thermal diffusivity of the gas.

For deployments with sodium-azide-based inflators, the exhaust gas is primarily nitrogen, and ν, k, c_p, and Pr are available in tabular form as a function of temperature (*e.g.,* Incropera and Dewitt 1985). The objective of these calculations is to obtain an average Nu as a function of Re for the prescribed geometry, which effectively gives h as a function of u. Martin presents data relating Re to $Nu/Pr^{0.42}$ for a range of geometries. The important geometric parameters are expressed nondimensionally as H/D, the ratio of the orifice-to-surface distance to the jet diameter, and r/D, the ratio of the radius of the circular surface area over which Nu is averaged to the jet diameter.

The geometric ratio of r/D has a strong effect on $Nu/Pr^{0.42}$. The effect of increasing r/D is to reduce the average Nu, indicating a reduction in average h. This is readily apparent geometrically, since the area over which Nu is averaged increases with the square of r. The ratio H/D has a fairly small effect (± 10%) over a range of H from 2 to 10 diameters. Martin presents a graph of correction factors to be used when H/D differs from a nominal 7.5.

For a single, round, impinging jet, the empirical data take the form

$$Nu/Pr^{0.42} = c\, Re^{n}$$

where c and n are constants. Using the data presented in Martin (1977), an empirical function for the case of H/D =7.5 and r/D = 1 is

$$Nu/Pr^{0.42} = 0.6233\, Re^{0.5409}.$$

Using the definitions of Nu, Pr, and Re, the average heat transfer coefficient to the skin may be estimated as a function of impinging jet velocity and airbag vent geometry:

$$h = \left(\frac{k}{D}\right) Pr^{0.42}\, 0.6233 \left(\frac{u\,D}{\nu_f}\right)^{0.5409}. \tag{11}$$

The gas characteristics are evaluated at the film temperature, which is defined to be the average of the surface and free-stream temperatures. The gas jet diameter (D) is the effective diameter of the exhaust port and is determined by the airbag exhaust port diameter and orifice coefficient.

4.1.2.2 Solution of Fourier Equation for Semi-Infinite Solid under Surface Convection. Henriques and Moritz demonstrated that heat transfer into the skin can be modeled using a semi-infinite-solid assumption with epidermis parameters. Their experiments used contact with the skin by hot objects that could reasonably be expected to bring the skin surface temperature immediately to the temperature of the contacting object. A closed-form solution to the Fourier heat equation (equation 3) was used to obtain the temperature distribution in the skin as a function of time.

In the current research, the surface convection raises the skin surface temperature over time, necessitating a different set of boundary conditions and a different solution to the Fourier equation. During an airbag deployment, the exhaust gas exits the vent ports with time-varying temperature and velocity, suggesting that time-varying boundary conditions at the skin surface would be appropriate. However, since solution methods for time-varying boundary conditions are considerably more complex, a constant-convection-coefficient assumption was used. Under this assumption, a closed-form solution to the Fourier equation (Incropera and DeWitt 1985) can be expressed as

$$\frac{T(x,t)-T_i}{T_\infty - T_i} = \operatorname{erfc}\left(\frac{x}{2\sqrt{\alpha t}}\right) - \left[\exp\left(\frac{hx}{k}+\frac{h^2\alpha t}{k^2}\right)\right]\left[\operatorname{erfc}\left(\frac{x}{2\sqrt{\alpha t}}+\frac{h\sqrt{\alpha t}}{k}\right)\right], \qquad (12)$$

where T_i is the initial (constant) skin temperature, T_∞ is the impinging gas temperature, h is the heat transfer coefficient ($W/m^2/K$), $\operatorname{erfc}(w) = 1 - \theta(w)$, and the remaining terms are defined as in equation (5), above.

Equation (12) is used to calculate the temperature distribution in the skin as a hot gas jet impinges on the surface. The temperature at the basal epidermal layer as a function of time is calculated using this function, with the free-stream temperature and heat transfer coefficient as independent variables.

In the Henriques and Moritz experiments, the cooling-off period immediately following the application of heat was short relative to the exposure duration, and was consequently not considered as part of the interval during which the skin temperature was elevated. In the case of airbag exhaust gas exposure, the time required for the skin at the critical depth to cool below the temperature at which thermal injury can occur can be substantially longer than the exposure duration. This is because the high gas temperatures and high heat transfer coefficients create large temperature gradients at the skin surface. After the gas flow has stopped, the temperature at the basal epidermal layer remains elevated until the heat that has been transferred to the outer layers of skin has been conducted deeper into the skin or removed through passive convection at the skin surface.

To account for injury that may occur during this cooling interval, a second heat-transfer phase was added. The boundary conditions for this phase are similar, except that the heat transfer coefficient at the skin surface is much smaller (for passive convection) and the heat transfer is out of the skin (to the cooler ambient air). A major difference between phases one and two is that the initial condition for phase 1 consists of a constant temperature in the skin, while the initial condition for phase two is determined by the

temperature distribution at the end of phase one, which is described by equation (12) using t equal to the exposure duration.

Because of the more complicated initial condition for phase two, a closed-form solution to the heat equation is not available. Instead, the temperature distribution is approximated by a Fourier-series solution consisting of forty cosine terms with appropriate coefficients. Appendix A includes a description of the Fourier-series solution procedure. Since the primary mechanism by which heat is transferred from the basal epidermal layer is by conduction into the dermis, the thermal properties of the dermis rather than epidermis were used in phase two calculations. The resulting function is used to obtain the temperature history at the critical skin depth for the second phase of heat transfer.

Figures 13 and 14 show the predicted temperature distribution in the skin over time for a threshold-duration heat gun exposure (150 ms) at 450 °C and 53 m/s. An interesting observation is that the temperature at the critical skin depth (72 μm) continues to increase for a short period of time following the end of the exposure, as the heat in the outer layers of epidermis is conducted inward. Figure 15 shows the temperature at the critical skin depth (72 μm) from the exposure described in Figures 13 and 14.

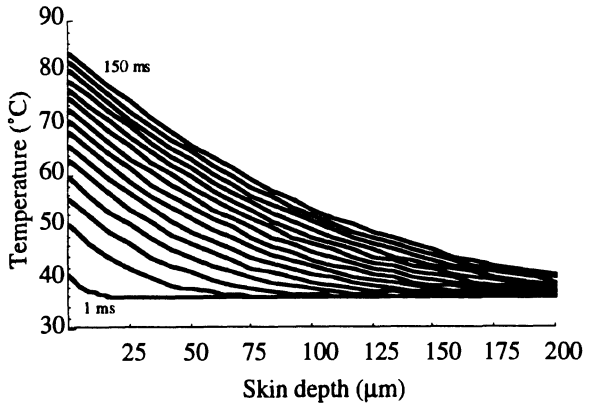

Figure 13. Predicted temperature in the skin as a function of skin depth during a 150-ms, 450 °C, 66-m/s heat gun exposure. Temperature curves are separated by 10 ms.

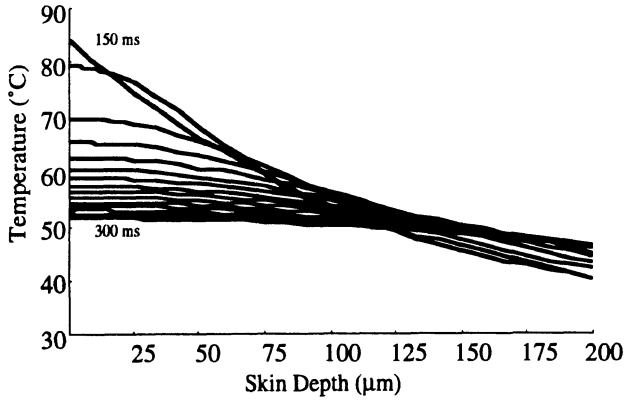

Figure 14. Predicted temperature in the skin as a function of skin depth immediately following a 150-ms, 450 °C, 66-m/s heat gun exposure. Temperature curves are separated by 10 ms.

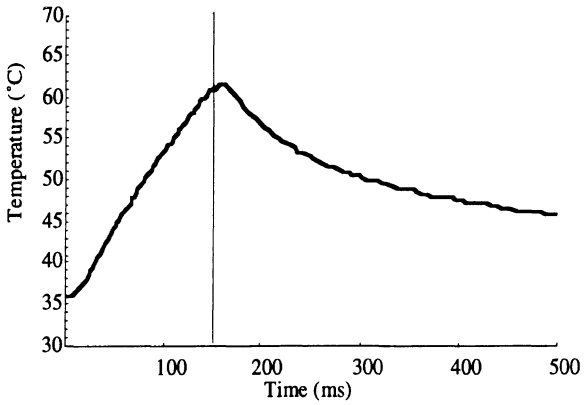

Figure 15. Predicted temperature at the critical skin depth (72 μm) during and immediately following a 150-ms, 450 °C, 66-m/s heat gun exposure. Vertical line indicates the end of the hot gas flow.

4.1.2.3 Prediction of Burn Using Omega Injury Function. The mathematical model described above is used to calculate the temperature history at the basal epidermal layer (critical skin depth) for any combination of constant impinging gas temperature, composition, velocity, and exposure duration. Equation (8) is then used to calculate Ω. If $\Omega > 1$, then a transepidermal burn is predicted. In contrast, if $\Omega < 1$, then no burn (or a first-degree burn) is predicted.

Henriques (1947) suggests that a value of $\Omega = 0.53$ can be taken to be the threshold for first-degree burn (erythema with no cell necrosis), but fewer data are available for that threshold. Because of the method used to obtain the formula for Ω (see Section 4.1.1.3 above), values of Ω other than 0.53 and 1 have no physical meaning. Thus, an exposure resulting in $\Omega = 2$ is not twice as severe as an exposure producing $\Omega = 1$.

However, the injury function can be used to calculate a range of injury severities by using the depth of cell necrosis as the index of severity. A burn is more severe if cell necrosis has progressed to a deeper level. A useful technique is to calculate Ω for a range of cell depths to identify maximum depth at which $\Omega > 1$. However, for the purposes of the current research, Ω is calculated only for the estimated depth of the basal epidermal layer to obtain the threshold for partial-thickness skin burn.

4.1.3 Comparison of the Analytic Burn Injury Model with the Human Burn Injury Data

In the heat-gun experiments with human subjects, fourteen data points consisting of air temperature, air velocity, and burn-threshold exposure duration were obtained. The analytic burn model described above was exercised with the gas temperature and velocity for each of these points to compare the model predictions with the experimental findings. The heat gun exit diameter of 10 mm was used as the gas jet diameter. The distance from the heat gun exit to the skin surface was about 40 mm, so H/D was about 4. A correction factor of 0.94 was obtained from the graph in Martin (1977) and applied to the value of h obtained by equation (11). A search procedure was used to determine the threshold exposure duration that would correspond to $\Omega = 1$. With the gas temperature and velocity set, Ω was calculated at 5-ms intervals until the shortest exposure duration that produced $\Omega > 1$ was obtained.

The predicted threshold exposure durations were, on average, about 60 ms shorter than the threshold exposure durations obtained with the heat gun. After careful assessment of potential error sources, an additional correction factor of 0.6 was applied to the empirical heat transfer coefficient calculation to produce better agreement between the model predictions and the human-subject data. Figure 16 shows the model predictions with and without the correction factor for each of the fourteen exposure-duration thresholds obtained in the heat gun experiments.

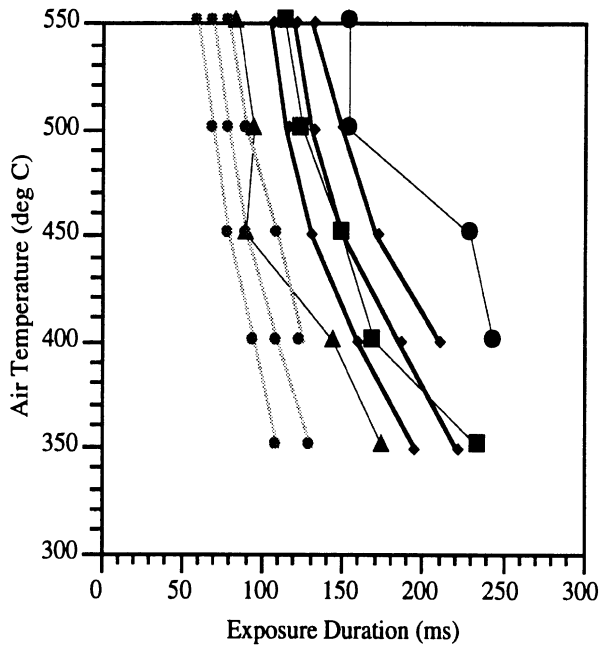

Figure 16. Comparison of heat gun data and initial analytical model predictions. Human-subject data are shown as in Figure 6. Gray lines indicate model predictions for heat-gun test conditions without correction factor. Model predictions with correction factor are shown with thick lines and ◆ symbols.

As with the heat gun data, the model predictions can also be described well by an exponential function:

$$t = \mathrm{Exp}[\, 7.20 - 0.0132\, u - 0.00363T + 1.23 \times 10^{-5}\, uT]. \qquad (13)$$

Figure 17 shows both exponential functions, equations (2) and (13), as three-dimensional surfaces. In general, the analytical burn injury model predicts a smaller effect of velocity on the exposure-duration thresholds than was observed in heat-gun testing.

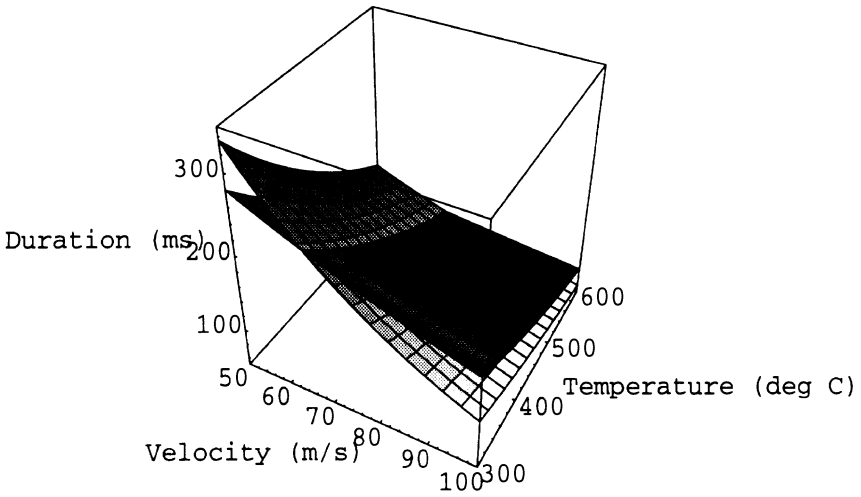

Figure 17. Comparison of exponential fits to human burn threshold data obtained with the heat gun and analytical model predictions. Lighter surface is exponential fit to heat-gun data.

4.2 AIRBAG INFLATION MODEL

As illustrated in Section 2, measurements of airbag exhaust gas temperature and velocity are not easily made, and are subject to potentially large errors. In view of these difficulties, another method of obtaining information on these characteristics of airbag exhaust gases was sought. One approach is to use the measured performance of the airbag inflator and the airbag characteristics, along with an analytical gas dynamics model, to predict the exhaust temperature and velocity. A lumped-parameter, isentropic flow model presented by Wang and Nefske (1988), Wang (1989), and Wang (1991) was adapted for this purpose. There are many other possible model formulations, including many more sophisticated techniques, that could be used to obtain the desired information on gas flow. The Wang model was selected because it was computationally tractable on the computing equipment readily available, and because it held the promise of producing useful results with a manageable amount of model manipulation. The Wang model is described more thoroughly in Appendix B. This overview will serve to illustrate the use of the model in predicting exhaust characteristics of interest.

4.2.1 Overview of Airbag Inflation Model

The airbag system consists of an inflator and an airbag, which may have vent holes and/or porous fabric. The inflator performance is determined by reference to inflator tank-test data. The inflator is mounted on a sealed, 1-ft^3 tank and fired into the tank. The resulting pressure rise in the tank is recorded and used as descriptive data for that inflator

design. As Wang (1991) has noted, the tank pressure alone is insufficient to specify the inflator performance for use with vented airbags. One other piece of information (*e.g.*, the mass flow rate from the inflator or the gas temperature in the tank) is needed to fully describe the inflator performance. Appendix B contains a discussion on obtaining the appropriate data from an inflator tank test. For this discussion, the tank internal pressure and inflator mass flow rate, both as a function of time, are assumed to be available.

The airbag inflation takes place in two stages. In the first stage, the pressure in the airbag is assumed to be atmospheric. Gas flow from the inflator increases the volume of the airbag until the nominal volume (*e.g.*, 60-L) is attained. Since there is no pressure differential across the airbag vent ports, no exhaust gas flow occurs during the first stage. In the second stage, the pressure rises in the airbag as the fabric pulls tight (and stretches, if desired), and gas begins to flow from the vent ports. The exhaust gas velocity is determined primarily by the pressure in the airbag. High internal airbag pressures result in high exhaust gas velocities. In this lumped-parameter model, the pressure and temperature in the airbag are uniform, and the gas velocity through the vent ports and fabric is also uniform. Since the model is isentropic, there is no exchange of energy between the gas and the airbag, *i.e.*, no momentum or heat transfer. A full discussion of the model formulation is found in Appendix B.

4.2.2 Predictions of Airbag Inflation Model

The airbag inflation model was exercised using tank-test data from five inflators as input, and with the following assumptions:

1. 60-L nominal airbag volume
2. No fabric stretch
3. No occupant interaction
4. Two 35-mm vent ports
5. No fabric leakage
6. Vent port orifice coefficient = 0.6

The nominal airbag volume is typical of driver-side airbags. Fabric stretch would tend to increase the volume of the airbag, thereby decreasing the internal pressure and decreasing the exhaust gas velocity. Occupant interaction can dramatically increase the airbag internal pressure and exhaust gas velocity, but, since data on occupant interaction were not available, no interaction was assumed. The 35-mm vent ports are also typical for current driver-side airbags. Assuming no fabric leakage is conservative because the predicted airbag internal pressures will be higher than otherwise. The vent port orifice coefficient is a very important term, both because it has a strong effect on the predicted exhaust velocity and because it determines the effective diameter of the exhaust gas jet. The gas jet diameter is an important parameter in the heat transfer coefficient calculations.

Figures 18, 19, and 20 show airbag internal pressure, exhaust gas velocity, and exhaust gas temperature predictions for five inflators identified by their nominal peak tank-test pressure. In each of the plots, the curve peak ranking corresponds to the ranking of the five inflator tank-test peaks: 560, 475, 420, 350, and 320 kPa.

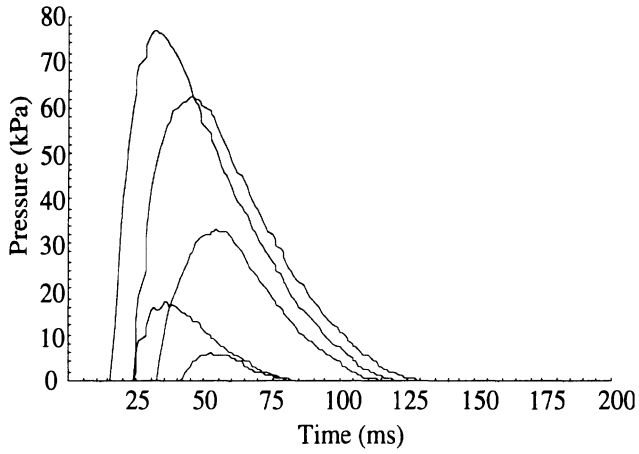

Figure 18. Predicted internal airbag pressure for five inflators.
Curve peak ranking corresponds to tank-test peak ranking:
560, 475, 420, 350, and 320 kPa.

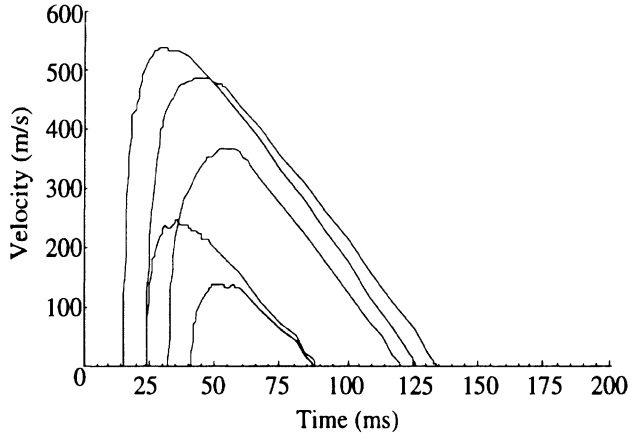

Figure 19. Predicted exhaust gas velocity for five inflators.
Curve peak ranking corresponds to tank-test peak ranking:
560, 475, 420, 350, and 320 kPa.

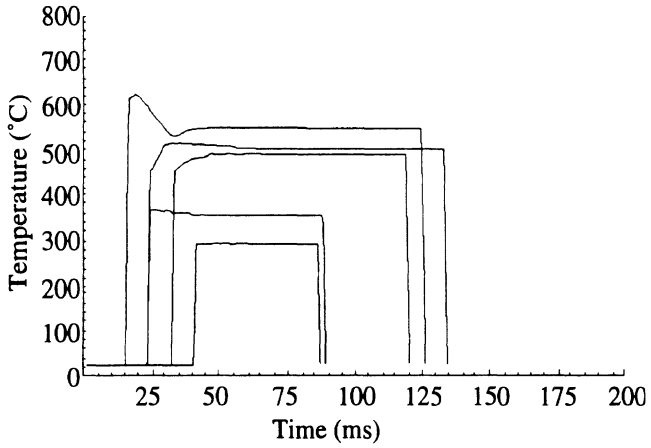

Figure 20. Predicted exhaust gas temperature for five inflators.
Temperature is assumed to return to ambient immediately after gas flow stops.
Curve peak ranking corresponds to tank-test peak ranking:
560, 475, 420, 350, and 320 kPa.

4.3 INTEGRATION OF AIRBAG INFLATION AND BURN INJURY MODELS

Figure 21 shows the information flow in the engineering process of assessing the burn potential of an airbag system. The inputs to the model are the specifications of the airbag system. These include the inflator tank-test pressure curve, the inflator mass flow curve, the nominal airbag volume, the vent port geometry, the fabric stretch factor, and the fabric leakage factor. The composition of the inflation gas is also important. For sodium azide inflators, the inflation gas can be assumed to be nitrogen. The inflation model is used to calculate the airbag exhaust gas temperature and velocity as a function of time.

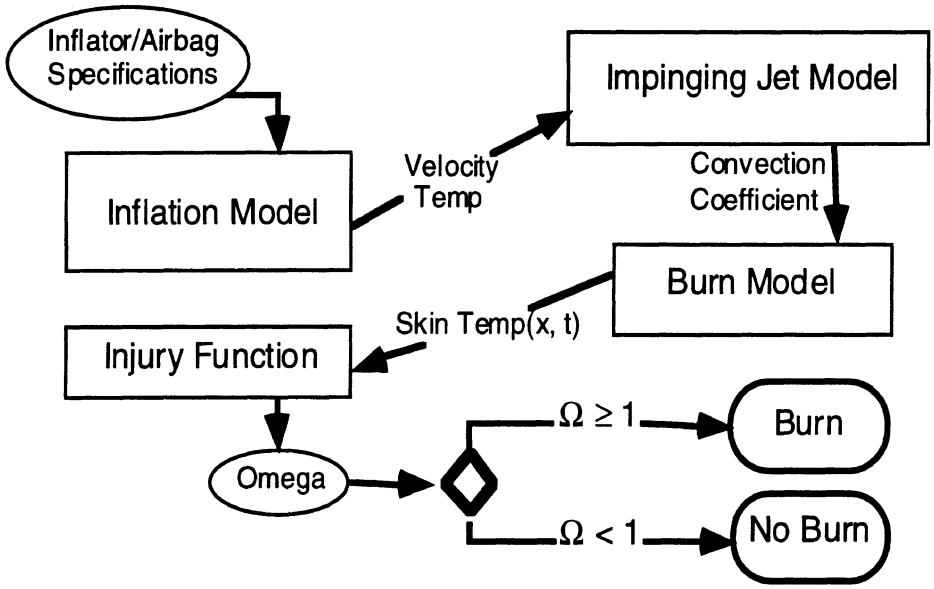

Figure 21. Information flow in process of predicting convection burn from airbag and inflator specifications.

Estimates of the average gas temperature and velocity are used to determine a constant heat transfer coefficient for use in the burn model. The impinging jet model consists of the empirical formulation provided by Martin (1977) and expressed in equation (11). The average temperature over the period of gas flow through the vent ports is used to calculate appropriate gas properties and as the free-stream temperature for the burn model. A representative velocity is calculated by squaring the average square root of the velocity over the period of gas flow. This gives a number slightly lower than would be obtained using the arithmetic average and is more appropriate given the formula for the heat transfer coefficient in which the velocity appears in approximately square-root form.

The structure of the empirical relationship used to determine the heat transfer coefficient produces a counter-intuitive result with respect to the effect of gas jet diameter on the heat transfer coefficient. Figure 22 shows the heat transfer coefficient for air at 400 °C plotted as a function of velocity for five jet diameters. The mathematical relationship among the convection coefficient, velocity, and diameter is

$$h = C \frac{u^{0.5409}}{D^{(1-0.5409)}}, \tag{14}$$

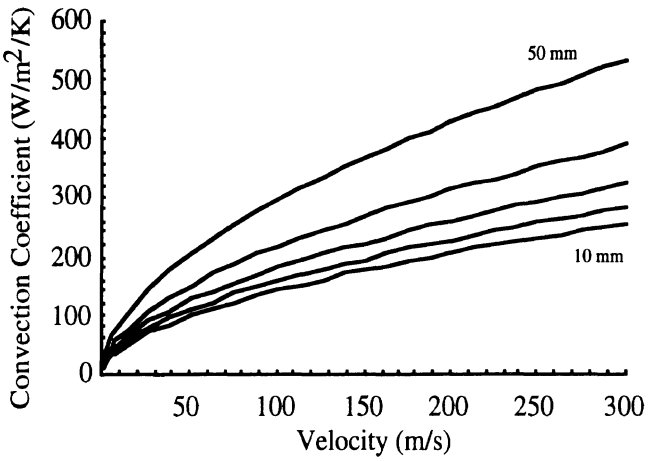

Figure 22. Relationship between velocity and gas jet diameter in determining convection coefficient. Values shown are for air at 400 °C.

As an approximation, the convection coefficient is related, via a proportionality function determined by gas parameters, directly to the square root of velocity and inversely to the square root of diameter. Thus, increasing the jet diameter *reduces* the heat transfer coefficient.

This result is counterintuitive because we expect that the larger jet will carry a larger quantity of heat to the skin surface, resulting in more heat transfer. Under the model formulation, the heat transfer coefficient calculated is the average convection coefficient over a circular area with a diameter twice the diameter of the jet. Therefore, a larger diameter jet transfers more heat to the skin over the (larger) area of interest, but the transfer per unit area is lower. Using a constant target area for different jet diameters is not practical because different empirical formulae are used for different relative target sizes. Further, there is only a small increase in average heat transfer coefficient when the relative target size is reduced below r/D = 1.

The physical explanation for the reduction in convection coefficient with increasing jet diameter is that the thermal boundary layer thickness is proportional to the square root of the jet diameter. A larger jet produces a thicker boundary layer, and so the heat transfer is slower. This observation has important implications for airbag design. Based on the current analysis, a single large vent port may be less likely to cause burns than several smaller vent ports with the same effective area (the product of the area and orifice coefficient). Further study is necessary to verify this effect for the velocities and diameters of interest.

Another unexpected finding resulting from the relationship between velocity and diameter is that the experimental test conditions used with human subjects (velocities between 50 and 100 m/s, 10-mm-diameter air jet) produce heat transfer coefficients similar to those produced by airbags (velocities between 200 and 500 m/s, diameters between 30 and 50 mm). This similarity increases confidence in the applicability of the human-subject burn data to airbag deployment conditions.

The thickness of the epidermis is also important in determining the shortest exposure duration that will cause a burn. Falstie-Jensen *et al.* (1988) reported that the standard deviation of epidermal thickness for 10 adult males was 16 μm over five body areas, including the inside of the upper arm. Figure 23 shows model predictions for critical

skin depth values of 38 and 102 μm, corresponding to the mean value of 70 ± 2 standard deviations. Data collected with the heat gun are also shown in Figure 23. Based on these model simulations, variance in skin thickness can be expected to affect sensitivity to short-duration convection burn substantially.

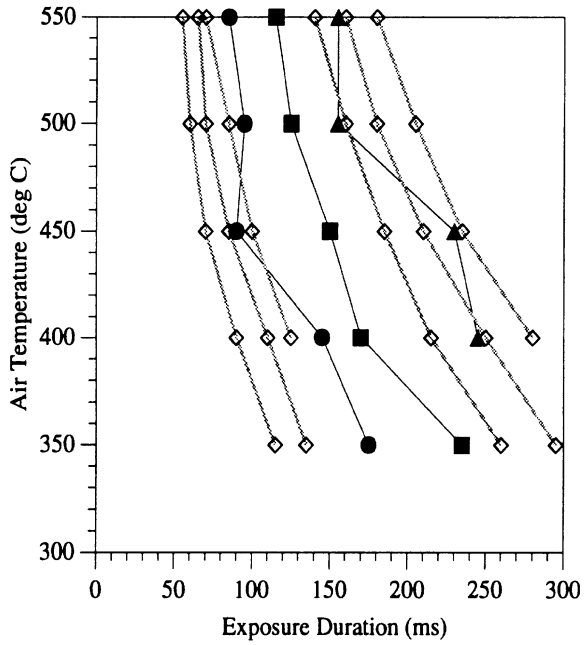

Figure 23. Comparison of model predictions (◇ symbols) using epidermal thickness equal to the mean ± 2 s.d. (11) and the heat gun data.

5.0 DISCUSSION AND CONCLUSIONS

Skin burn threshold data obtained through human-subject testing show clear trends with respect to the effects of temperature and velocity changes on the burn threshold. The desire to minimize the discomfort of the subjects, and the constraints imposed by the heat gun design, restricted the range of temperatures and velocities that could be investigated. Nonetheless, the threshold exposure duration was found to decrease with increasing temperature and increasing velocity, as expected. The primary limitations of these data are related to the small sample size and potential errors in characterizing the test conditions. Data from two subjects were used to obtain two of the threshold exposure durations (see Table 2), while the remainder were obtained from individual subjects. Because of the large predicted effect of epidermal thickness on the burn threshold (see Figure 23), considerable scatter due to intersubject variability might have been observed if multiple subjects had been tested at each condition. Although the temperature measurements were probably quite accurate (± 10 °C), there is less confidence in the velocity measurements. There was reasonable agreement between the two measurement methods used, but the accuracy may not be better than ±10%. Such an error would result in a change of about 10 ms in the burn threshold predicted by the analytical burn model, which is not a substantial deviation.

The mathematical model used to predict the temperature distribution in the skin was adapted from previous burn research. The primary contributions of the current work are the addition of a convection boundary condition, development of a two-phase solution, and validation through human-subject experiments.

Few of the model parameter values are known with great precision. The effect of the epidermal thickness on the model predictions has been discussed above. The thermal diffusivity of the skin was calculated using data from Henriques and Moritz (1947) for juvenile pig skin. Based on the similar morphology of pig and human skin, these values are believed to be reasonable to describe the thermal characteristics of human skin. However, there is substantial variation in these parameters among individuals and at different body sites. In addition, the water content of the skin, particularly the outer epidermal layers, has a strong influence on the thermal properties. High water content increases thermal conductivity, although it also increases the heat capacity. In addition, even a light film of moisture on the skin (*e.g.,* sweat) can substantially increase the amount of heat that must be conducted to the skin to produce a burn.

The choice of continuous solutions to the Fourier equation was made for computational simplicity. A finite difference method that could include appropriate thermal characteristics for both the epidermis and dermis is feasible and should be explored in future work. Such methods would allow, for example, time-varying gas temperatures and heat transfer coefficients. Although there are methods for continuous solutions under those conditions, they are difficult to implement programmatically.

The greatest uncertainty in modeling the heat transfer to the skin is in the calculation of the heat transfer coefficient using empirical correlation data. The circular, perpendicularly impinging jet was chosen for the heat gun testing and for airbag burn modeling because it produces a thin boundary layer and high heat transfer rates compared to other geometries. The correlational data available in Martin (1977) were obtained from several sources that provide reasonably consistent values for heat transfer coefficients in the velocity range of interest. However, as noted above, the expected

accuracy of the correlational method is only about 25 percent. Since the correction factor applied to the model to obtain a better fit to the experimental data is only 40 percent, we conclude that the analytical model provides a good match to the experimental data within the expected range of error in parameter estimates. When the potential variability in epidermal thickness is considered, the correspondence between the heat gun data and the model predictions is remarkable. We do not assume that this correspondence implies that our parameter estimates are necessarily correct: it is likely that there are offsetting errors in a number of estimates. However, for purposes of predicting short-duration convection burns, the analytical model appears to work well.

An important question is to what extent the analytical model should be used. The approach to airbag assessment described above uses the analytical model in its entirety to determine the potential for a convection burn from airbag exhaust gas. An alternative is to use the human-subject data directly, bypassing the heat transfer calculations. However, these data must be scaled according to the diameter of the impinging gas jet to be modeled. Currently, the only method available to do that scaling is the empirical correlation formula used to calculate the heat transfer coefficient.

The analytical model can be used to examine the potential depth (severity) of a burn, as well as to investigate the effects of, for example, epidermal thickness. Further, the effects of changes in gas composition that may result from changes in inflator propellants can be explored. Consequently, further development and validation of the analytical burn injury model is warranted.

The most important component of the burn injury model is the omega burn injury function. This function was developed by Henriques (1947) from contact burn threshold data and is based on the observation that burn injury shows the essential characteristics of a rate process. To use the omega injury function for short-duration events, it is necessary to assume that the chemical processes responsible for burn injury are the same for 200-ms and 200-second exposures, which is plausible but by no means certain. The primary limitation of the current use of the omega function is the extrapolation of the Henriques and Moritz (1947) data, which were obtained with exposure durations greater than 300 seconds, to burn events lasting less than one second. Small errors in the eight data points used to determine the omega function coefficients could result in large errors in the threshold estimates for short-duration exposures. For example, a one-percent change in the ΔE value results in a 20-ms shift in the threshold values predicted by the analytical model for the heat gun test conditions.

Parameter values for the omega function were determined by experiments in which the temperature at the critical skin depth was known. Since it is impractical to measure the temperature at the basal epidermal layer, contact burns produced by relatively long exposures, for which the temperature at the basal epidermal layer will be almost exactly the (known) temperature of the skin surface, are the best source of data. A larger data set of this type would allow a more precise determination of the omega parameter values, which would increase confidence in the analytical burn model predictions.

The lumped-parameter, isentropic flow model described above is a useful means of obtaining estimates of the airbag exhaust gas velocity and temperature. Although other, more sophisticated models are also available, the Wang model produces usable predictions that, in conjunction with the analytical burn model, have been shown in other experiments to be predictive of the burn potential of driver-side airbag systems.

One of the most important parameters in the gas dynamics model is the vent port orifice coefficient. We have assumed in our analyses that there is no gas leakage through the

fabric or seams. This is a conservative assumption, since fabric leakage would tend to lower the airbag internal pressure and reduce the velocity of the gas escaping through the vents. The orifice coefficient multiplied by the vent port area gives the effective area of the vent port; that is, the area of the neck of the gas jet passing through the port. The flow through a straightedged orifice narrows substantially just beyond the orifice edge, reducing the effective size of the orifice. The choice of orifice coefficient affects the model predictions in two ways. Smaller orifice coefficients reduce the effective vent area, thereby increasing the predicted internal airbag pressure. Since the exhaust gas velocity is determined primarily by the internal airbag pressure, smaller orifice coefficients result in higher gas velocities and can produce longer exposure durations since the inflation gas takes longer to escape.

Smaller orifice coefficients also produce smaller gas jet diameters for purposes of burn injury modeling. The effective gas jet diameter is the product of the vent port diameter and the square root of the orifice coefficient. Smaller gas jets produce higher heat transfer coefficients. Therefore, under the model assumptions, a smaller orifice coefficient will decrease the exposure duration that will produce a burn since the heat transfer coefficient will be higher because of increased velocity and reduced gas jet diameter.

Because the orifice coefficient is such a critical parameter, an effort should be made to estimate the value experimentally for a particular airbag design. The model prediction that is most readily compared to experimental data is the airbag internal pressure. Although there is considerable variance in deployments, even with nominally identical airbags, adjusting the orifice coefficient to produce accurate airbag internal pressure predictions is one way to improve the performance of the gas dynamics model. Since the exhaust gas velocity predictions are primarily dependent on the airbag internal pressure, confidence in the velocity predictions will also be increased by validating the internal pressure predictions and adjusting the vent port orifice coefficient appropriately.

The burn model is currently implemented using a fixed distance from the vent port to the skin surface of four port diameters. For a typical airbag vent port of 35 mm, this represents a distance of 140 mm. This is a reasonable distance between the vent port and a driver's arm during a deployment, although both shorter and longer distances are also likely in the field. The heat transfer coefficient predictions for distances between 2 and 10 diameters are within a ±10% range, because the lateral diffusion of the gas jet within that distance range is minimal at velocities of interest (> 100 m/s). Consequently, calculations at a single distance are reasonable in assessing the burn potential of airbags.

The influence of occupant interaction with the airbag on the risk of burn injury has not yet been thoroughly examined. Occupant interaction will increase the internal pressure substantially, thereby increasing the exhaust gas velocity and increasing the heat transfer coefficient. The magnitude of the effect may be limited if the pressure differential across the vent port during occupant ridedown is sufficient to induce choked flow, which will limit the exit velocity of the gas. Calculating the choked flow velocity for the vent port will allow an estimate of the upper limit of the heat transfer coefficient. However, as with the orifice coefficient determination, airbag internal pressure measurement during dynamic testing with dummies is an appropriate way to determine more realistic vent port gas velocities. Preliminary studies indicate that the exit velocities during occupant ridedown are substantially higher than during static testing, increasing the risk of burn injury. Occupant interaction issues will be examined in future research using both computerized modeling and dynamic testing.

6.0 REFERENCES

Falstie-Jensen, N., Spaun, E., Brochner-Mortensen, J., Falstie-Jensen, S. (1988). The influence of epidermal thickness on transcutaneous oxygen pressure measurements in normal persons. *Scandinavian Journal of Clinical and Laboratory Investigations*, 48:519-523.

Fox, R.W., and McDonald, A.T. (1985). *Introduction to Fluid Mechanics.* New York: Wiley.

Henriques , F.C. (1947). Studies of Thermal Injury. V. The predictability and the significance of thermally induced rate processes leading to irreversible epidermal injury. *Archives of Pathology*, 43:489–502.

Henriques , F.C., and Moritz, A.R. (1947). Studies of Thermal Injury. I. The conduction of heat to and through the skin and the temperatures attained therein. A theoretical and an experimental investigation. *American Journal of Pathology*, 23:531-549.

Huelke, D.F., Roberts, J.V., and Moore, J.L. (1993). Air bags in crashes: clinical studies from field investigations. *Proc. 13th International Technical Conference on Experimental Safety Vehicles*, pp. 140-148. U.S. Department of Transportation, National Highway Traffic Safety Administration, Washington, D.C.

Incropera, F.P., and DeWitt, D.P. (1985). *Introduction to Heat Transfer.* New York: Wiley.

Martin, H. (1977). Heat and mass transfer between impinging gas jets and solid surfaces. *Advances in Heat Transfer*, 13:1–60.

Meyer, W., Schwarz, R., and Neurand, K. (1978). The skin of domestic animals as a model for the human skin, with special reference to the domestic pig. *Current Problems in Dermatology*, 7:39–52.

Moritz, A.R. (1947). Studies of Thermal Injury. III. The pathology and pathogenesis of cutaneous burns. An experimental study. *American Journal of P*athology, 23:915–941.

Moritz, A.R., and Henriques , F.C. (1947). Studies of Thermal Injury. II. The relative importance of time and surface temperature in the causation oaf cutaneous burns. *American Journal of Pathology,* 23:695–720.

Pinsky, M.A. (1991). *Partial Differential Equations and Boundary Value Problems with Applications.* New York: McGraw-Hill.

Reinfurt, D.W., Green, A.W., Campbell, B.J., and Williams, A.F. (1993). *Survey of attitudes of drivers in air bag deployment crashes. Technical Report.* Insurance Institute for Highway Safety, Arlington, VA.

Wang, J.T., and Nefske, D.J. (1988). *A new CAL3D airbag inflation model.* SAE Technical Paper No. 880654. Warrendale, PA: Society of Automotive Engineers.

Wang, J.T. (1989). Recent advances in modeling of pyrotechnic inflators for inflatable restraint systems. *ASME Pub.* AMD Vol. 106 and BED Vol. 13:89–93.

Wang, J.T. (1991). *Are tank pressure curves sufficient to discriminate airbag inflators?* SAE Technical Paper No. 910808. Warrendale, PA:Society of Automotive Engineers.

Wolfram, S. (1993). *Mathematica: A System for Doing Mathematics by Computer.* New York: Addison Wesley.

Zawacki, B.E. (1987). The local effects of burn injury. In Boswick, J.A. (ed). *The Art and Science of Burn Care.* Rockville, MD: Aspen Publishers.

APPENDIX A:
MATHEMATICAL MODEL OF CONVECTION BURN INJURY

A.1 HEAT TRANSFER COEFFICIENT

In order to determine the rate of heat transfer to the skin surface due to the airbag exhaust gas, we must first calculate a heat transfer coefficient. The exhaust gas exiting the airbag at an exhaust port and striking the skin surface is modeled as a round gas jet impinging perpendicularly onto an infinite plane surface, as shown in Figure A1.

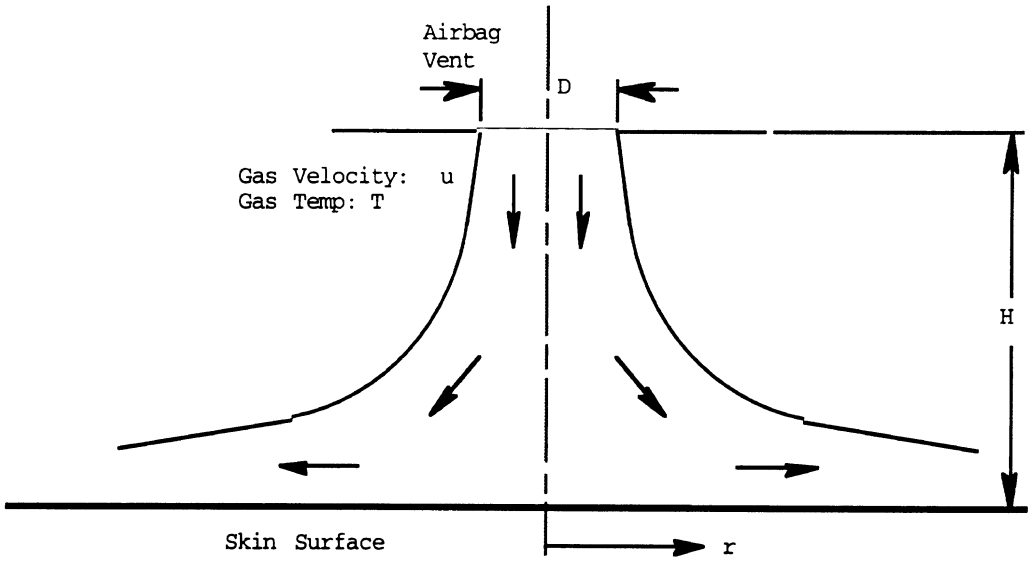

Figure A1. Impinging jet geometry.

Martin (1977) reported empirical correlations relating the Reynolds number (Re) to a ratio of Nusselt (Nu) to Prandtl (Pr) numbers for this geometry. These dimensionless parameters are defined as follows:

$$Re = \frac{uD}{\nu} \tag{1a}$$

$$Nu = \frac{hD}{k} \tag{1b}$$

$$Pr = \frac{\nu_f}{\alpha} \tag{1c}$$

where

u is the gas jet free-stream velocity,
r is the radius of target area,
D is the vent diameter,
ν is the kinematic viscosity of the gas at the free-stream temperature,
ν_f is the kinematic viscosity of the gas at the film temperature,
k is the thermal conductivity of the gas,
h is the heat transfer coefficient from the gas to the surface, and
$\alpha = \frac{k}{\rho c_p}$, the thermal diffusivity of the gas.

Values for the parameters ν, k, c_p, and Pr are available in tabular form as a function of temperature and gas composition from many sources (*e.g.*, Incropera and Dewitt 1985). To obtain the heat transfer coefficient, it is necessary to calculate an average Nu as a function of Re for the prescribed geometry, which effectively gives h as a function of u. Martin (1977) presents data relating Re to $Nu/Pr^{0.42}$ for a range of geometries. The important geometric parameters are expressed nondimensionally as H/D, the ratio of the orifice-to-surface distance to the jet diameter, and r/D, the ratio of the radius of the circular surface area over which Nu is averaged to the jet diameter.

The geometric ratio of r/D has a strong effect on $Nu/Pr^{0.42}$. The effect of increasing r/D is to reduce the average Nu, indicating a reduction in average h. This is readily apparent geometrically, since the area over which Nu is averaged increases with the square of r, while D is fixed. For airbag burn analysis, it is reasonable to take r/D = 1, meaning that the target diameter is equal to twice the diameter of the jet. The H/D ratio has a much smaller effect, typically less than 10 percent for r/D ratios between 0.5 and 10.

Martin presents data obtained for single round jets with the geometric ratio H/D equal to 7.5 and r/D equal to 1. For a single, round, impinging jet, the empirical data take the form

$$Nu/Pr^{0.42} = c\,Re^{n} \tag{2}$$

where c and n are constants. Using the Martin data, an empirical function for H/D = 7.5 and r/D = 1 is

$$Nu/Pr^{0.42} = 0.6233\,Re^{0.5409}. \tag{3}$$

Using the definitions of Nu, Pr, and Re, the average heat transfer coefficient to the skin may be estimated as a function of impinging jet velocity and airbag vent geometry.

$$h = \left(\frac{k}{D}\right) Pr^{0.42}\; 0.6233 \left(\frac{u\,D}{\nu_f}\right)^{0.5409}. \tag{4}$$

The gas characteristics are evaluated at the film temperature, which is defined to be the average of the surface and free-stream temperatures. The gas jet diameter (D) is the effective diameter of the exhaust port and is determined by the airbag exhaust port diameter and orifice coefficient.

A.2 HEAT TRANSFER TO THE SKIN

The next step in the injury modeling process is to determine the temperature of the skin as a function of time during the thermal insult. Henriques and Moritz (1947), in studies with porcine and human skin, have validated a semi-infinite-solid approximation model for heat transfer to the skin. This approximation will be used here.

In general, one-dimensional heat flow can be described by the Fourier heat equation

$$\frac{\partial^2 T}{\partial x^2} = \frac{1}{\alpha_s}\frac{\partial T}{\partial t} \tag{5}$$

where T(x, t) is the skin temperature at depth x and time t, and α_s is the thermal diffusivity of the skin. The objective of this analysis is to determine the time-dependent temperature at some critical skin depth. Basal epidermal depth is chosen as the skin depth of interest because the temperature at this skin depth is the determinant of the threshold of second-degree burn. While epidermal thickness varies widely across the body, 72 μm is a reasonable approximation (Falstie-Jensen *et al.* 1988).

Heat transfer to the skin is divided into two sequential phases with different initial conditions and boundary conditions. For each phase, the temperature at some depth L (selected to approximate infinite depth -- about 1.5 mm is adequate for these calculations) remains constant at the initial skin temperature T_i. The other boundary condition is set according to the prevailing heat transfer rate at the surface. For the first phase, during which high-temperature gas is impinging on the surface, the surface heat transfer rate is determined by the convection coefficient calculated using equation (4). For the second phase, the surface boundary condition is set to approximate passive convection from the skin surface to the ambient air during the period immediately following hot-gas flow.

Table A1
Phases of Heat Transfer to Skin

Phase	Event	Boundary Conditions	Initial Conditions
1	High-Temperature Gas Flow	$T_{(L,t)} = T_i$ $-k \left.\frac{\partial T}{\partial x}\right\|_{x=0} = h[T_\infty - T_{(0,t)}]$	$T_{(x,0)} = T_i$
2	Ambient Temperature (immediately after gas flow)	$T_{(L,t)} = T_i$ $-k \left.\frac{\partial T}{\partial x}\right\|_{x=0} = -q$ (small)	$T_{(x,0)} = \left. T_{(x,t)}\right\|_{t = \text{end Phase 1}}$

A.3 SOLUTION METHOD

Phase 1

For the first phase, a closed-form solution to equation (5) is available (Incropera and DeWitt 1985). With boundary and initial conditions as shown in Table A1, the temperature distribution in the skin is given by

$$\frac{T(x,t) - T_i}{T_\infty - T_i} = \theta_c\left(\frac{x}{2\sqrt{\alpha t}}\right) - \left[\exp\left(\frac{hx}{k} + \frac{h^2\alpha t}{k^2}\right)\right]\left[\theta_c\left(\frac{x}{2\sqrt{\alpha t}} + \frac{h\sqrt{\alpha t}}{k}\right)\right], \qquad (6)$$

where

T_i is the initial (constant) skin temperature,
T_∞ is the impinging gas temperature,
h is the heat transfer coefficient,
k is the thermal conductivity of the skin,
ρ is the density of the skin,
c_p is the heat capacity of the skin,
$\alpha_s = \frac{k}{\rho c_p}$ is the thermal diffusivity,

$\theta(w) \equiv \frac{2}{\sqrt{\pi}} \int_0^w e^{-v^2}\, dv$ is the Gaussian error function,

and $\theta_c(w) = 1 - \theta(w)$.

Note that the skin temperature over x (depth) is assumed to be constant at the start of the burn event, and that the heat transfer coefficient remains constant throughout the exposure.

Phase 2

The second-phase computations are made more complicated by the intial conditions, which are determined by the temperature distribution in the skin at the end of the first phase. The Fourier heat equation is solved using a Fourier series approximation. See Pinsky (1991) for a discussion of this solution method.

For the second phase, the problem is to solve the heat equation subject to non-homogeneous boundary conditions (*i.e.*, not equal to zero) with an initial, nonconstant temperature distribution v(x):

$$\frac{\partial^2 T}{\partial x^2} = \frac{1}{\alpha_s}\frac{\partial T}{\partial t} \qquad (7a)$$

with boundary conditions for $t > 0$

$$T(L,t) = T_i \qquad (7b)$$

$$-k\left.\frac{\partial T}{\partial x}\right|_{x=0} = q \qquad (7c)$$

and initial condition for $0 < x < L$

$$T(x, 0) = v(x). \tag{7d}$$

The desired solution T(x, t) may be decomposed into two parts: a steady-state solution, U(x), and a transient solution v(x, t), so that

$$T(x,t) = U(x) + v(x,t). \tag{8}$$

For $t \to \infty$, $\partial T/\partial t \to 0$ and (7a) becomes

$$\frac{\partial^2 T}{\partial x^2} = 0. \tag{9}$$

A general solution to (7a) is of the form Ax + B, where A and B are constants. Applying boundary conditions (7b-c), we obtain

$$U(x) = -\frac{qx}{k} + T_i + \frac{qL}{k} \tag{10}$$

as steady state solution. Applying the substitution in (8) to the original problem, we now have an initial condition problem with homogeneous boundary conditions, as follows:

$$\frac{\partial^2 v}{\partial x^2} = \frac{1}{\alpha_s}\frac{\partial v}{\partial t} \tag{11a}$$

with boundary conditions for $t > 0$

$$v_{(L,t)} = 0 \tag{11b}$$

$$-k\left.\frac{\partial v}{\partial x}\right|_{x=0} = 0 \tag{11c}$$

and initial condition for $0 < x < L$

$$v(x, 0) = v(x) - U(x) \tag{11d}$$

where v(x,t) is a new function defined by

$$v(x,t) = T(x,t) - U(x). \tag{12}$$

Note that for $t = 0$, $v(x,t) = v(x)$. We now solve this modified problem using the method of separation of variables. We first assume that $v(x, t) = X(t)T(t)$. Substituting into (11a) we obtain

$$X''(x)T(t) = \alpha T'(t)X(t)$$

or, separating variables,

$$\frac{X''(x)}{X(x)} = \frac{T'(t)}{\alpha T(t)} = K \tag{13}$$

where K is a constant eigenvalue. From (13) we can obtain two ordinary differential equations

$$X''(x) - KX(x) = 0 \tag{14a}$$

and

$$T'(t) - \alpha KT(t) = 0. \tag{14b}$$

To determine a value of K, we first consider (14a) along with the (now homogeneous) boundary conditions. A general solution to (14a) has the form

$$X(x) = C_1 \cos\left[\sqrt{-K}x\right] + C_2 \sin\left[\sqrt{-K}x\right] \tag{15}$$

where C_1 and C_2 are constants. Under the boundary condition (11c),

$$C_2\sqrt{-K} = 0$$

so $C_2 = 0$. (Values of $K \geq 0$ are neglected since they result only in constant or trivial solutions.) Then, under (11b),

$$X(L) = C_1 \cos\left[\sqrt{-K}L\right] = 0,$$

which, since $C_1 > 0$, is true for $\sqrt{-K}L = (n - \frac{1}{2})\pi$, where $n = 1, 2, 3, \ldots$,

$$K = -\left[\left(n - \tfrac{1}{2}\right)\frac{\pi}{L}\right]^2.$$

So,

$$X_n(x) = c_n f_n(x) \tag{16}$$

where c_n is a constant and

$$f_n(x) = \cos\left[\left(n - \tfrac{1}{2}\right)\frac{\pi x}{L}\right]$$

are the eigenfunctions of the problem. The solution to (14b) is then of the form

$$T_n(t) = b_n \exp[-K\alpha t] = b_n \exp\left[\left[\left(n - \tfrac{1}{2}\right)\frac{\pi}{L}\right]^2 \alpha t\right]. \tag{17}$$

Combining (16 and 17), a general solution of (11) is

$$v(x,t) = \sum_{n=1}^{\infty} A_n \exp\left[\left[\left(n - \tfrac{1}{2}\right)\frac{\pi}{L}\right]^2 \alpha t\right] \cos\left[\left(n - \tfrac{1}{2}\right)\frac{\pi x}{L}\right]), \tag{18}$$

where the A_n are constant coefficients. The coefficients A_n are determined by expanding the initial condition (17d) into the series of eigenfunctions such that the solution satisfies the initial conditions. The A_n are chosen such that the function $A_n f_n(x)$, n = 1, 2, 3 ... is the projection of the initial conditions onto the orthogonal set $f_n(x)$ over the interval $0 \leq x \leq L$. The A_n are calculated by

$$A_n = \frac{\int_0^L [\, v(x) - U(x)] \, f_n(x)\, dx}{\int_0^L [\, f_n(x)]^2 \, dx} \tag{19}$$

which is equivalent to the inner product of the initial conditions and the eigenfunction divided by the norm of the eigenfunction. The temperature distribution T(x,t) is then given by (13) to be

$$T(x,t) = -\frac{qx}{k} + Ti + \frac{qL}{k} + \sum_{n=1}^{\infty} A_n \exp\left[\left[\left(n-\tfrac{1}{2}\right)\frac{\pi}{L}\right]^2 \alpha t\right] \cos\left[\left(n-\tfrac{1}{2}\right)\frac{\pi x}{L}\right]. \tag{20}$$

The number of Fourier series terms necessary to obtain suitable convergence is dependent on the initial conditions. Because of the sharp gradient near x = 0 at the start of the second phase, the second-phase calculations typically require 40 terms. From the two-phase solutions, a function is obtained for the temperature at the critical depth (nominally 72 μm). This skin temperature function is used to evaluate the integral injury function.

A.4 INTEGRAL INJURY FUNCTION

Henriques (1947) demonstrated that burn injury could be treated as a rate process in which the progression of the injury is related both to the temperature and the duration of exposure. This relationship can be expressed by the integral equation

$$\Omega = G \int_0^t e^{\left(\frac{-\Delta E}{R\,T(t)}\right)} dt \qquad (21)$$

where

Ω is the injury parameter,

R is the universal gas constant ($8.3144 \frac{J}{mol\ K}$)

T(t) is the temperature at the basal epidermal layer as a function of time (K), and G and ΔE are empirically determined constants.

Henriques (1947) calculated the parameters G and ΔE using contact-burn data from tests with pigs and graphical fitting techniques. The values identified by Henriques (1947) are $G = 3.1 \times 10^{98}\ s^{-1}$, and $\Delta E = 629 \times 10^3$ J/mol. The value of R used by Henriques was 2 cal/mol/K, or 8.374 J/mol. A more accurate value of R is 8.3144 J/mol/K. In equation (21), the coefficient of T is $1/(\Delta E/R)$, so the appropriate value of ΔE is dependent on the value of R used. Taking R as 8.3144 J/mol/K, the recalculated parameter values are $G = 3.1 \times 10^{98}\ s^{-1}$, and $\Delta E = 623580$ J/mol.

Fitting equation (21) to experimental data requires specifying an arbitrary value of Ω to correspond to a particular injury threshold. Henriques chose the threshold of full epidermal necrosis to assign $\Omega \equiv 1$. Using the same values for G and ΔE, a value of $\Omega = 0.53$ was found to correspond to the threshold of epidermal injury. In relation to more commonly used descriptions of burn severity, $\Omega = 0.53$ corresponds to the threshold of first-degree burn. $\Omega = 1$ corresponds to a minimum-severity, partial-skin-loss burn, in which the depth of injury has extended fully through the epidermis.

APPENDIX B:
MATHEMATICAL MODEL OF AIRBAG INFLATION

B.1 BACKGROUND

The gas-dynamics model described in this appendix was adapted from Wang and Nefske (1988), Wang (1989), and Wang (1991). This model was chosen to demonstrate how the burn injury model could be used with mathematical models of airbag inflation to predict burn. Other models that have increased fidelity may provide more accurate assessments, but the Wang model provides useful airbag performance predictions that can be verified with laboratory measurements and is readily used with the burn injury model.

B.2 NOTATION

In the equations to follow, subscripts associate variables with various parts of the airbag system, as follows:

$[]_T$	Tank Test
$[]_1$	Inflator
$[]_2$	Airbag
$[]_3$	Atmosphere at Exhaust Vents

B.3 INFLATOR MASS FLOW

From the standard inflator tank test, the mass flow rate from the inflator into the tank may be determined as a function of time:

$$\dot{m}_{1T} = \frac{\dot{P}_T V_T}{k R T_1} \tag{1}$$

where

k is the ratio of specific heats (assumed to be nitrogen: $k = 1.4$),

$\dot{m}_{1T}$ is the time rate of change of mass in tank = inflator mass flow rate ($\frac{kg}{s}$),

$\dot{P}_T$ is the time rate of change of pressure in tank ($\frac{Pa}{s}$),

R is the gas constant (assumed nitrogen: $R = 296.8 \frac{J}{kg \cdot K}$),

T_1 is the temperature of gas in inflator, and

V_T is the volume of test tank (typically 1 ft^3 = 0.0283 m^3).

Because it is generally impractical to measure the temperature of the inflator gas directly, a "dual pressure" method of determining the inflator mass flow during the tank test has been developed (Wang 1989). Using P_1, the internal inflator pressure, and assuming choked flow, the mass flow rate from the inflator to the tank, $\dot{m}_{1T}$, can be calculated as follows:

$$\dot{m}_{1T} = \left(\frac{kC_{oa}^2 C_T^2}{RV_T}\right)\left(\frac{P_1^2}{\dot{P}_T}\right) \tag{2}$$

where

$C_{oa} = C_{1T} A_{1T}$,

C_{1T} is the inflator orifice coefficient,
A_{1T} is the inflator orifice area,

$$C_T = \left(2\left(\frac{kR}{k-1}\right)\left(\frac{2}{k+1}\right)^{\frac{1}{k-1}}\left(1 - \frac{2}{k+1}\right)\right)^{\frac{1}{2}}, \text{ and}$$

P_1 is the inflator pressure.

In practice, it is easiest to determine C_{oa} indirectly by considering an additional piece of information from the tank test. M is defined to be the total mass of gas that flows into the tank during the test. This can be determined by weighing the inflator before and after the test. Wang (1988) proposes another method of mass estimation involving consideration of the chemical reaction occuring in the inflator. C_{oa} can then be calculated by

$$C_{oa} = \left(\frac{MRV_T}{kC_T^2 P_{Int.}}\right)^{\frac{1}{2}} \tag{3}$$

where

$$P_{Int} = \int \frac{P_1^2}{\dot{P}_T}\, dt.$$

Since P_1 and $\dot{P}_T$ are measured during the tank test, the integral can be evaluated numerically to obtain a value for C_{oa}. The inflator mass flow rate as a function of time can then be calculated from equation (2). Consistent with the choked flow assumption, this mass flow rate will hold for all airbag pressures.

The inflator mass flow rate as a function of time will generally be available from the inflator manufacturer, who will use an analytical technique such as that described above to calculate the mass flow rate from data collected during tank tests. The calculation technique is described here for completeness and for application to situations in which the inflator mass flow rate may not be available directly.

B.4 AIRBAG INFLATION

The airbag inflation process consists of two phases. In the first phase, during which the airbag fills to its nominal volume, the pressure in the airbag is assumed to be atmospheric, yielding no mass flow through the vent ports or fabric. For the first phase,

$$\dot{V}_2 = \frac{V_T}{kP_a}\dot{P}_T \tag{4a}$$

$$\dot{m}_2 = \dot{m}_{1T} \tag{4b}$$

$$T_2 = \frac{P_a V_2}{m_2 R} \tag{4c}$$

$$P_2 = P_a \tag{4d}$$

Note that the volume of the airbag is directly proportional to the tank-test pressure. For the second phase, the pressure in the airbag rises above atmospheric, resulting in gas flow through the fabric and vents. During this phase,

$$\dot{m}_2 = \dot{m}_{1T} - \dot{m}_{23} \tag{5a}$$

$$\dot{P}_2 = \frac{V_T\dot{P}_T - kRT_2\dot{m}_{23} + kP_2\Delta\dot{V}}{V_2 + kP_2c_sV_{20}} \tag{5b}$$

$$\dot{V}_2 = \frac{c_sV_{20}\,(V_T\dot{P}_T - kRT_2\dot{m}_{23}) - V_2\Delta\dot{V}}{V_2 + kP_2c_sV_{20}} \tag{5c}$$

$$T_2 = \frac{P_2V_2}{m_2R} \tag{5d}$$

$$\dot{m}_{23} = C_{23}A_{23}\frac{P_2}{R\sqrt{T_2}}\left(\frac{P_e}{P_2}\right)^{\frac{1}{k}}\left[2\left(\frac{kR}{k-1}\right)\left(1-\left(\frac{P_e}{P_2}\right)^{\frac{k-1}{k}}\right)\right]^{\frac{1}{2}} \tag{5e}$$

where

P_e is the exhaust pressure in orifice (Pa),
C_{23} is the orifice coefficient for vents and fabric,
A_{23} is the area of vents and fabric leakage (m^2),
c_s is the fabric stretch factor ($\frac{m^2}{N}$),
V_{20} is the nominal airbag volume (m^3), and
$\Delta\dot{V}$ is the rate of change of airbag volume due to occupant interaction ($\frac{m^3}{s}$).

The preceding analysis will give the mass flow rate through the vents as a function of time, the airbag characteristics, and the inflator tank-test data. To obtain the velocity of the gas exiting the exhaust vents, equation (5e) can be rewritten as follows:

$$\dot{m}_{23} = C_{23}A_{23}\rho u \tag{6a}$$

where the density of the exhaust gas is

$$\rho = \frac{P_2}{RT_2}\left(\frac{P_e}{P_2}\right)^{\frac{1}{k}} \tag{6b}$$

and the velocity of the exhaust gas is

$$u = \left[2\,T_2 \left(\frac{kR}{k-1} \right) \left(1 - \left(\frac{P_e}{P_2} \right)^{\frac{k-1}{k}} \right) \right]^{\frac{1}{2}} \tag{6c}$$

The temperature of the exhaust gas can be readily determined for this isentropic process using the ideal gas relation

$$T_e = T_2 \left(\frac{P_e}{P_2} \right)^{\frac{k-1}{k}} \tag{7}$$

Thus, this lumped-parameter, isentropic airbag model gives the temperature and velocity of the airbag exhaust gas flow as a function of the inflator tank-test data and airbag properties.

APPENDIX C:
EXAMPLE CALCULATIONS FOR PREDICTING AIRBAG CONVECTION BURN INJURY

C.1 OVERVIEW

This appendix contains a step-by-step description of the process of predicting whether or not a driver-side airbag has the potential to cause a convection burn. Intermediate results are presented. The calculations were performed in *Mathematica* (Wolfram 1993) on Macintosh and Sun workstations.

Figure C1 shows an information-flow chart depicting the various types of data used in the model simulation and the sources of those data. Inflator tank-test data forms the basis of the gas-dynamics simulation of the airbag inflation process. Crash-victim simulation modeling can provide information on occupant interaction with the airbag, although, for this example, no occupant interaction is assumed. The airbag design parameter values can generally be obtained from the airbag manufacturer.

There are four mathematical submodels that are described in detail in Appendices A and B. The airbag inflation process is modeled using gas-dynamics equations provided by Wang (1988). This submodel produces predictions of exhaust gas velocity that are used with the Martin (1977) data to obtain a prediction of the convection coefficient at the skin surface. The exhaust gas temperature and heat transfer coefficient predictions are used with an adaptation of the Henriques and Moritiz (1947) heat transfer model to predict the temperature distribution in the skin during and immediately following hot-gas flow. Finally, the Henriques (1947) burn injury function is used with the predicted temperature history at the basal epidermal layer to determine whether the threshold for partial-thickness skin burn has been exceeded.

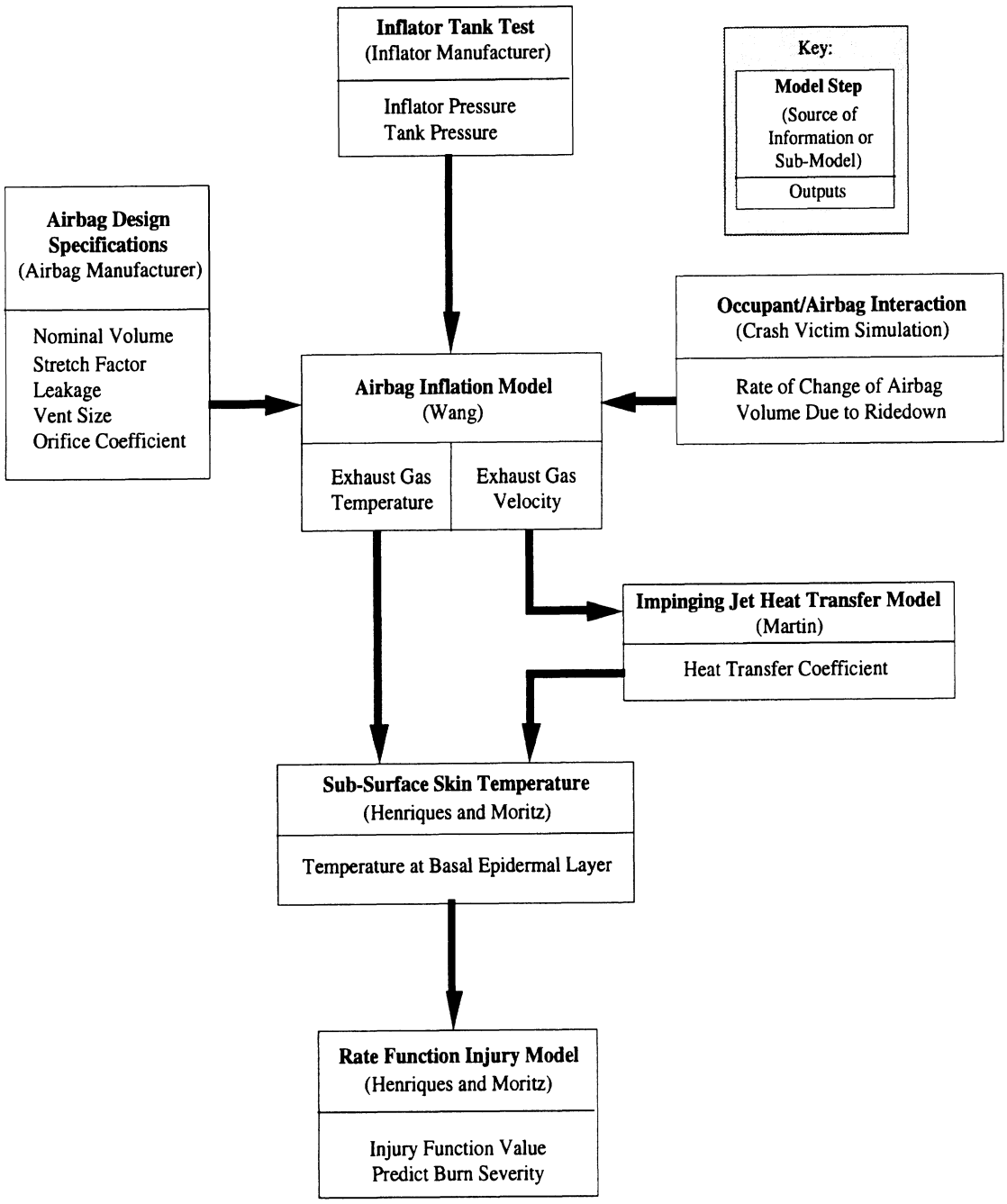

Figure C1. Schematic of burn-prediction process.

C.2 EXAMPLE CALCULATIONS

1. Obtain Inflator and Airbag Specification Data

The inflator is characterized by two data streams from the inflator tank test. Generally, the tank-test pressure and inflator mass flow rate are available from the manufacturer. For the current calculations, the data shown in Figures C2 and C3, obtained from a test with a 1-ft^3 tank, are used.

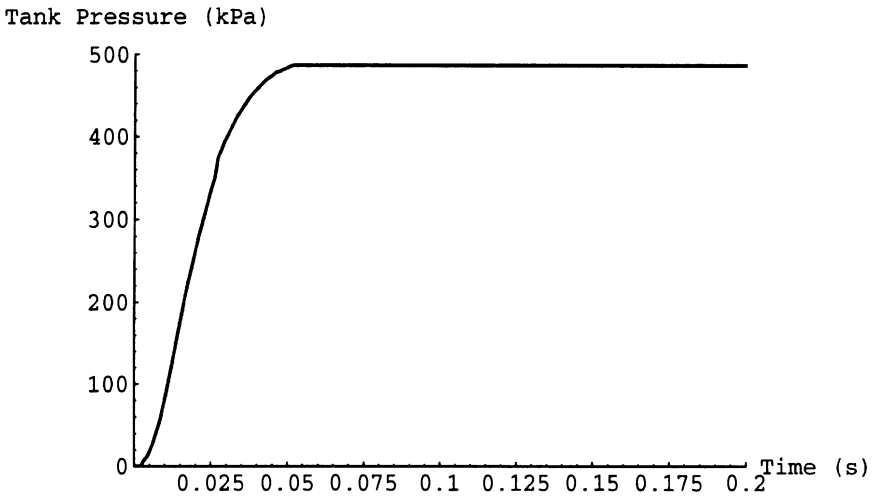

Figure C2. Inflator tank-test pressure curve.

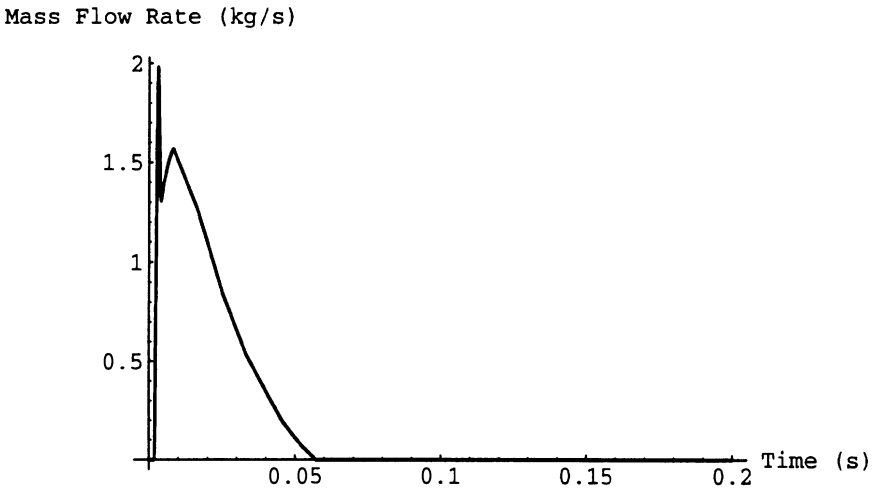

Figure C3. Inflator tank-test mass flow rate.

The following airbag specifications are used in these calculations:

a. 60-L nominal airbag volume,
b. no fabric stretch ($c_s = 0$),
c. no occupant interaction,
d. no fabric leakage (so that all gas escapes through vent ports,
e. airbag has two 35-mm vent ports with a total area of 0.00192423 m^2,
f. vent port orifice coefficient is 0.6, and
g. gas is N_2.

2. Exercise Gas Dynamics Model

Curves obtained for the airbag internal pressure, exhaust gas velocity, and exhaust gas temperature using the equations in Appendix B are shown in Figures C4, C5, and C6.

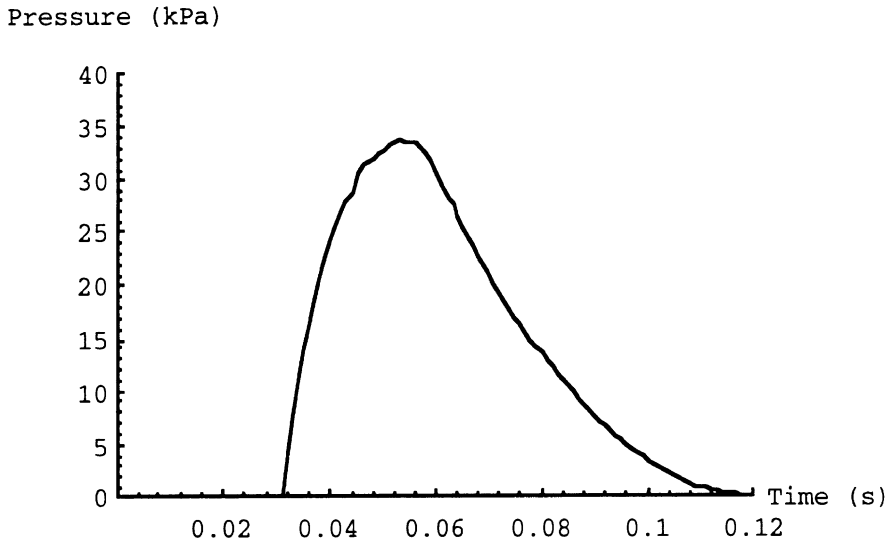

Figure C4. Airbag internal pressure predictions.

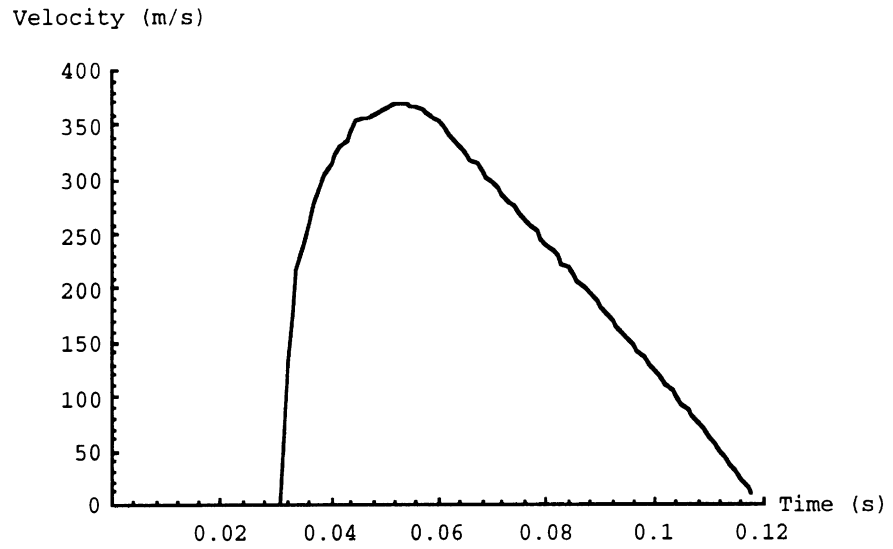

Figure C5. Airbag exhaust gas velocity predictions.

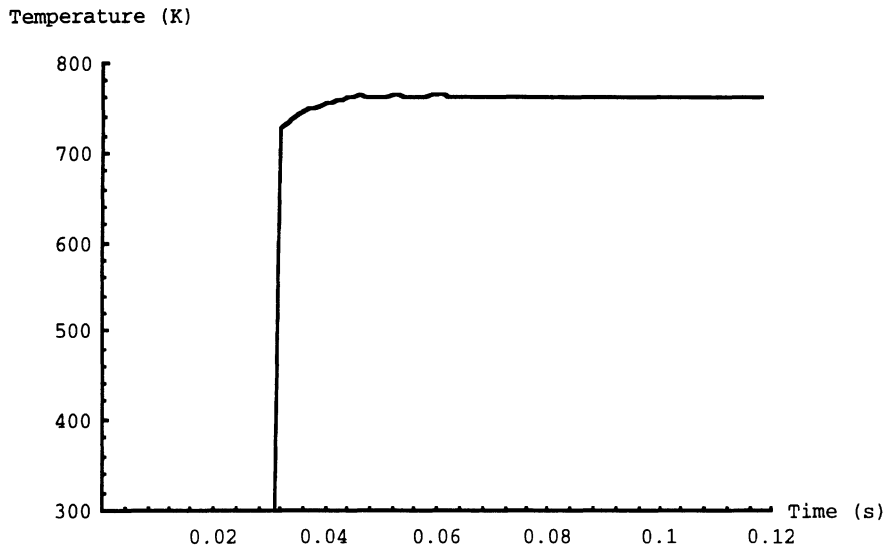

Figure C6. Airbag exhaust gas temperature predictions.

3. Calculate Constant Exhaust-Gas Temperature and Velocity Estimates

The burn injury model requires constant gas temperature and velocity as inputs. The exhaust gas temperature is obtained by averaging the temperature over the gas flow interval. The velocity estimate is obtained by computing the square of the average square root of the velocity. This method is used, rather than the arithmetic average, because the heat transfer coefficient is roughly proportional to the square root of velocity. Figures C7 and C8 show the constant velocity and temperature estimates along with the curves calculated above.

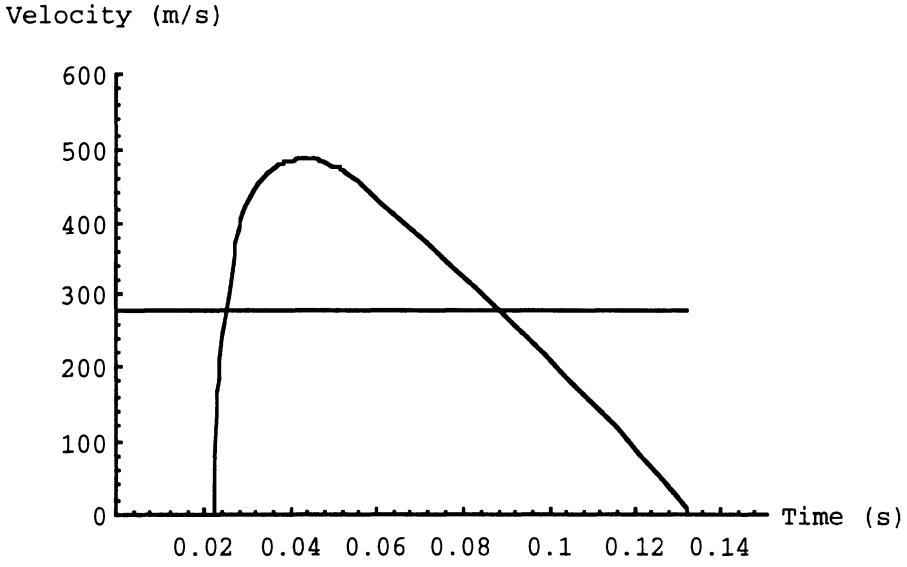

Figure C7. Exhaust gas velocity predictions and constant velocity estimate (278 m/s).

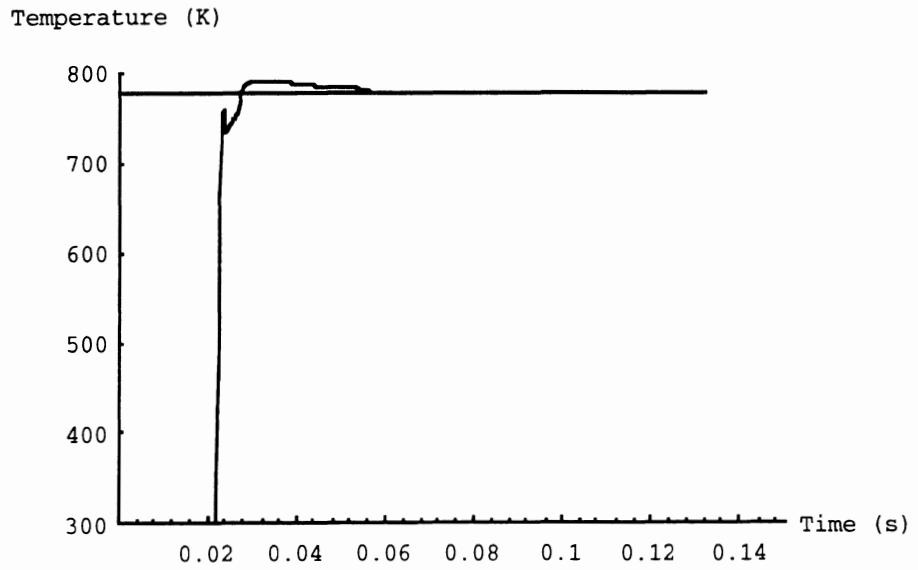

Figure C8. Exhaust gas temperature predictions and constant temperature estimate (778 K).

4. Calculate Skin Temperature Distribution

The heat transfer model described in Appendix A is then exercised using the gas jet characteristics determined in the last step (velocity = 278 m/s, temperature = 778 K). Table C1 shows the parameter values used with the heat transfer model.

Table C1
Heat Transfer Model Parameter Values

Parameter	Description	Value
k (epidermis)	Thermal conductivity	0.20949 W/m/K
k (dermis)	Thermal conductivity	0.3791 W/m/K
α (epidermis)	Thermal diffusivity	7.267×10^{-8}
α (dermis)	Thermal diffusivity	1.43×10^{-7}
Ti	Initial skin temperature	309 K
C_f	Heat transfer coefficient correction factor	0.6

Epidermis parameter values are used during the first phase, while dermis parameter values are used during the second phase. In the first-phase calculations, the exhaust gas temperature and velocity are used with the Martin (1977) empirical correlations to calculate the heat transfer coefficient. Because the gas parameter values are to be evaluated at the film temperature, which is defined to be the average of the surface and free-stream temperatures, an iterative procedure is used to determine the film temperature. The closed-form temperature distribution for the first phase is first calculated using gas parameters calculated assuming a fixed surface temperature of 350 K. The average predicted surface temperature is then obtained from the closed-form solution and used in a second iteration of the heat-transfer calculation. This process is repeated until the heat transfer coefficient estimate changes less than 2 $W/m^2/K$, which generally requires about four iterations. The heat transfer coefficient obtained in this example is 312 $W/m^2/K$.

Forty cosine terms are used with the Fourier solution for the second phase. A larger number of terms improves the convergence of the solution at the boundaries and for times near zero, but also increases computational requirements. A greater number of terms did not substantially change the injury function results for a number of typical burn injury simulations, so a function length of forty terms was chosen.

Figure C9 shows the temperature distribution in the skin after 20, 40, 60, 80, 100, and 109 ms of hot gas flow (end of phase 1). Figure C10 shows the temperature distribution in the skin 20, 40, 60, 80, 100, and 120 ms following the end of hot gas flow.

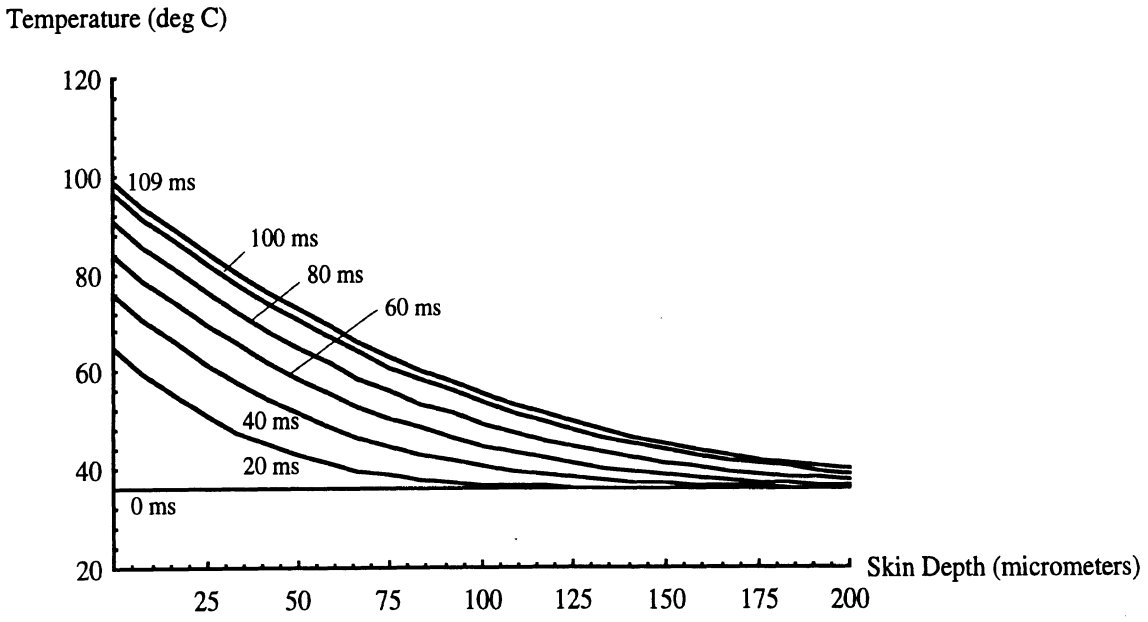

Figure C9. Temperature distribution in the skin during hot-gas flow (109 ms).

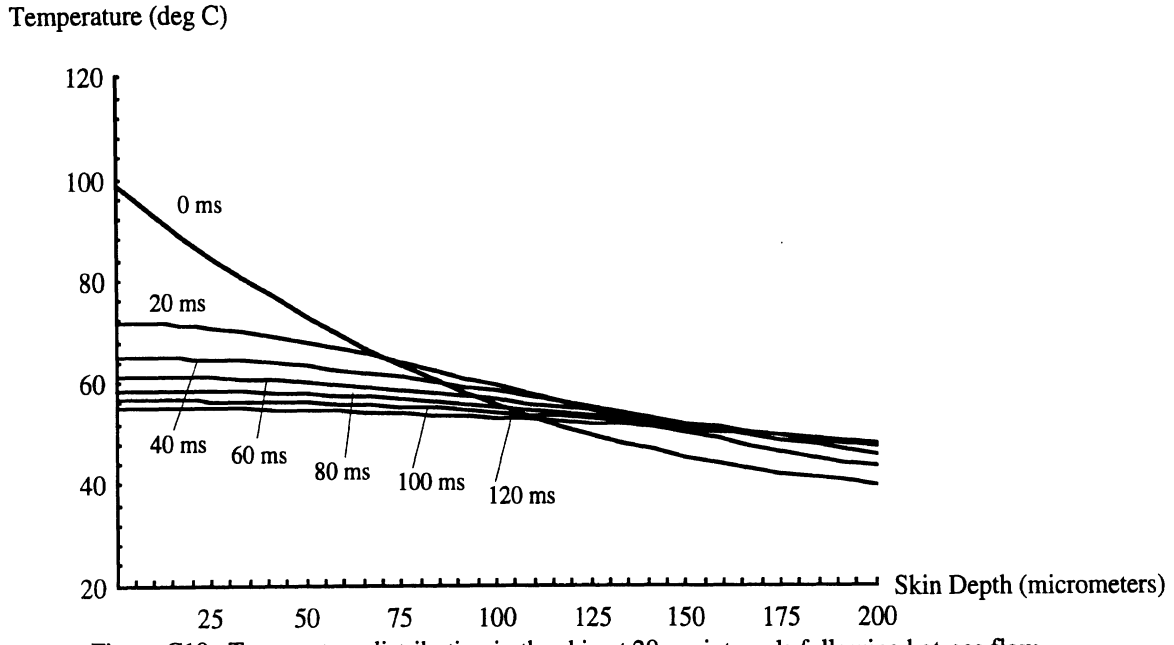

Figure C10. Temperature distribution in the skin at 20-ms intervals following hot-gas flow.

5. Calculate Omega Injury Parameter to Predict Burn

The temperature distributions for phase 1 and phase 2 are used to calculate the omega injury function value. The parameter values for this submodel are shown in Table C2.

Table C2
Burn Model Parameter Values

Parameter	Description	Value
G	omega function constant	3.1×10^{98}
ΔE	omega function activation energy	623580
d	critical cell depth	72×10^{-6} m

The temperature functions for phase 1 and phase 2 are solved for the temperature history at the critical skin depth of 72 μm, shown in Figure C11.

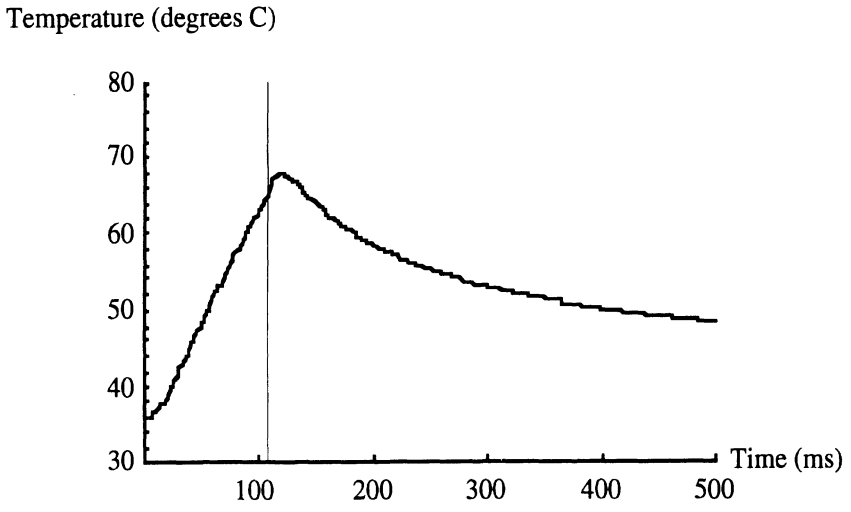

Figure C11. Temperature history at skin depth of 72 μm. Line indicates end of hot-gas flow.

The temperature history at the critical skin depth is used with the omega injury function. The value of Ω is 0.50 for phase 1 and 4.96 for phase 2, for a combined Ω of 5.46. Since $\Omega > 1$, skin burn is predicted.